of target genes, and it can elicit apoptosis by transcription-independent mechanisms (5, 28). Although apoptosis in response to p53 activation is often accompanied by caspase activation, the mechanisms underlying p53-induced caspase activation remain poorly understood. Caspase activities in RbAp48-induced apoptosis in HSG cells were assayed using a caspase family colorimetric substrate set. A significant increase in caspase 1 activity was detected with relatively elevated caspase 3 and 8 activity on RbAp48-induced apoptotic HSG cells (Fig. 4F). RbAp48-induced apoptosis in HSG cells was clearly inhibited by siRNA of E2F-1 and p53 but only moderately by siRNA of ARF (Fig. 4G).

RbAp48/E2F1/ARF-p53 pathway in the salivary glands. We evaluated the effects of RbAp48 overexpression and knockdown in primary MSG cells and documented the effects on E2F-1, ARF, and p53 protein levels in these cells. We demonstrated that overexpression of RbAp48 in MSG cells from B6 mice induced E2F-1, p19ARF, and phospho-p53 expression, and the inhibitory effect of siRNA of RbAp48 was observed from confocal microscopic analysis (Fig. 5A). We next examined whether TAM-induced apoptosis is associated with RbAp48 expression in MSG cells from B6 mice, compared with cells from $ER^{-/-}$, $E2F1^{-/-}$, and $p53^{-/-}$ mice. By confocal microscopic analysis, we found that TAM-induced apoptosis was associated with RbAp48 expression in MSG cells from B6 mice but not from $ER^{-/-}$, $E2F1^{-/-}$, and $p53^{-/-}$ mice Fig. (5B). We further examined the effect of OVX on the expression of RbAp48, E2F-1, p19ARF, and phospho-p53 in MSG cells from B6, $ER^{-/-}$, $E2F1^{-/-}$, and $p53^{-/-}$ mice. By double-labeled confocal microscopy, we found coexpression of RbAp48/E2F1, RbAp48/p19ARF, and RbAp48/p53 in MSG cells from OVX B6 mice but not from B6 mice (Fig. 5C). No differences in RbAp48/E2F1, RbAp48/p19ARF, and RbAp48/phospho-p53 expression levels were observed in MSG cells from non-OVX and OVX $ER^{-/-}$, $E2F1^{-/-}$, and $p53^{-/-}$ mice (Fig. 5C).

Findings in RbAp48-transgenic mice. We constructed several lines of B6 background TG mice (39) expressing RbAp48 in the salivary glands using Lama promoter as described in Materials and Methods. Prominent expression of RbAp48 in the salivary glands from TG mice was determined at the age of 8 to 20 weeks by both immunohistochemistry and Western blotting (Fig. 6A and B). No difference in RbAp48 expression in the spleen was observed between TG and WT mice. A considerable number of $TUNEL^+$ apoptotic epithelial duct cells were found in the salivary glands of RbAp48-TG mice but not WT mice at the age of 20 weeks (Fig. 6C). In addition, expression of E2F-1, p19ARF, and phospho-p53 was observed in the salivary glands of RbAp48-TG mice but not WT mice (Fig. 6D). BrdU studies of TG mice with ectopic RbAp48 in the salivary glands demonstrated that cellular proliferation is barely affected (Fig. 6E). No pathological findings were observed in other organs of TG mice.

DISCUSSION

In this study, we demonstrated the first evidence that gender-based, tissue-specific apoptosis could be induced in the exocrine gland cells through RbAp48 overexpression with p53 phosphorylation. Indeed, RbAp48 overexpression with apoptosis was observed in the exocrine glands in OVX C57BL/6 mice, and transgenic expression of the RbAp48 gene induced tissue-specific apoptosis in the exocrine glands.

RbAp48, initially identified as a retinoblastoma binding protein (34), was characterized as a component of distinct nucleosome-modifying complexes, including the nuclear histone deacetylases (18, 25). In general, the functions of the RbAp48-like proteins in these complexes remain undetermined. It was reported that E2F-1 and RbAp48 are physically associated in the presence of Rb and histone deacetylase (26), suggesting that RbAp48 could be involved in transcriptional repression of E2F-responsive genes. The induction of apoptosis in various cell lines is accompanied by a shift in Rb from the hyper- to the hypophosphorylated form (49). Rb dephosphorylation, which has been shown to be required for apoptosis, occurs in the early stage of apoptosis (6). Loss of Rb function can induce p53-dependent apoptosis, but little is known about the mechanisms of Rb-regulated p53-dependent apoptosis. Recently, Lieman et al. provided evidence for a novel mechanism linking Rb-E2F to the extrinsic apoptotic pathway through inactivation of focal adhesion kinase and activation of caspase 8 (20). It has been proposed that the E2F-1 transcription factor serves as a link between the Rb/E2F proliferation pathway and the p53 apoptosis pathway by inducing the expression of p14ARF, a protein that regulates p53 stability. Recent observations have revealed that p53 can directly translocate to mitochondria and induce apoptosis in a transactivation-independent manner (21). In this study, we confirmed a time-dependent downregulation of Mdm2, which is important as a regulatory partner of p53 (47). In addition to regulation of p53, Mdm2 has been reported to stimulate E2F-1 transactivation by a mechanism that remains unclear. E2F-1 can signal p53 phosphorylation in the absence of p14ARF, similar to the observed modifications to p53 in response to DNA damage. p53 modification is found to be crucial for E2F-1-mediated apoptosis, and this apoptosis is compromised when E2F-1 is coexpressed with a p53 mutant

pCMV-GFP, and then apoptosis was detected by PE-annexin V on GFP^+ cells. Infection of adenovirus β-galactosidase was used as a control. Graphs are representative of five independent experiments. (D) Expression levels of p53, phospho-p53 (Ser9), and Mdm2 in IPTG-treated RH0 cells. Other phosphorylated p53 proteins (Ser15, Ser20, and Ser392) were not detected. GAPDH expression was used for an internal control. Blots are representative of three independent experiments. (E) Detection of increased p21 expression, a major player in the p53-mediated pathway, by Western blotting. Blot is representative of two independent experiments. (F) Caspase activities of IPTG-treated RH0 cells were analyzed by a caspase enzymatic activity assay. A significant increase in caspase-1 activity was detected with relatively elevated caspase 3 and 8 activity. The absorbance of samples was read at 405 nm in a microtiter plate reader and the relative percent increase in activity was calculated by comparing the absorbance of IPTG-treated cells with that of untreated cells. Data are means ± standard deviations of triplicate samples. The graph is representative of three independent experiments. (G) RbAp48-induced apoptosis in HSG cells was clearly inhibited by siRNAs of E2F-1 and p53 but only moderately by siRNA of ARF. Graphs are representative of three independent experiments.

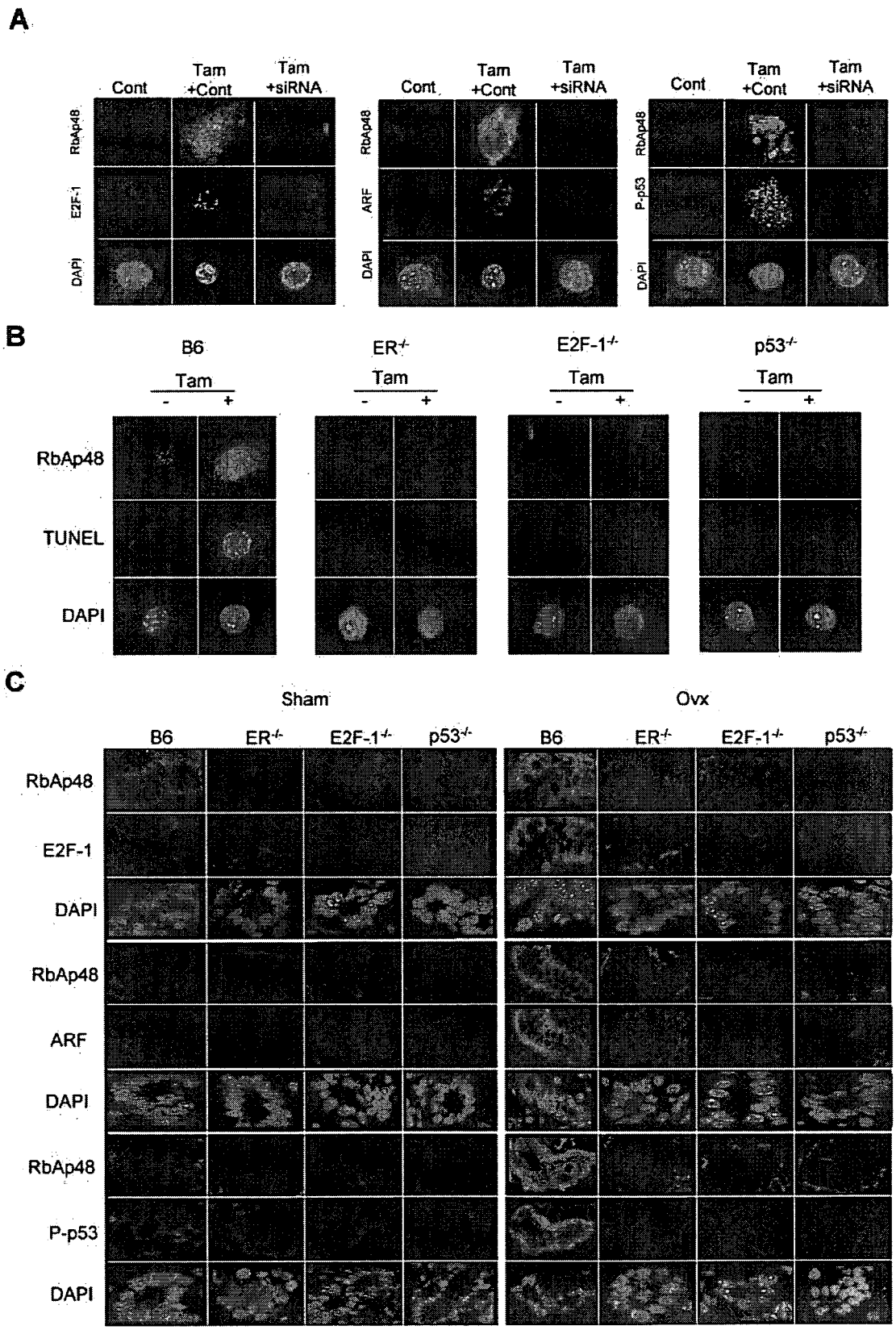
A
Cont
Tam +Cont
Tam +siRNA
RbAp48
E2F-1
DAPI
ARF
P-p53
B
B6
ER-/-
E2F-1-/-
p53-/-
Tam
-
+
TUNEL
C
Sham
Ovx

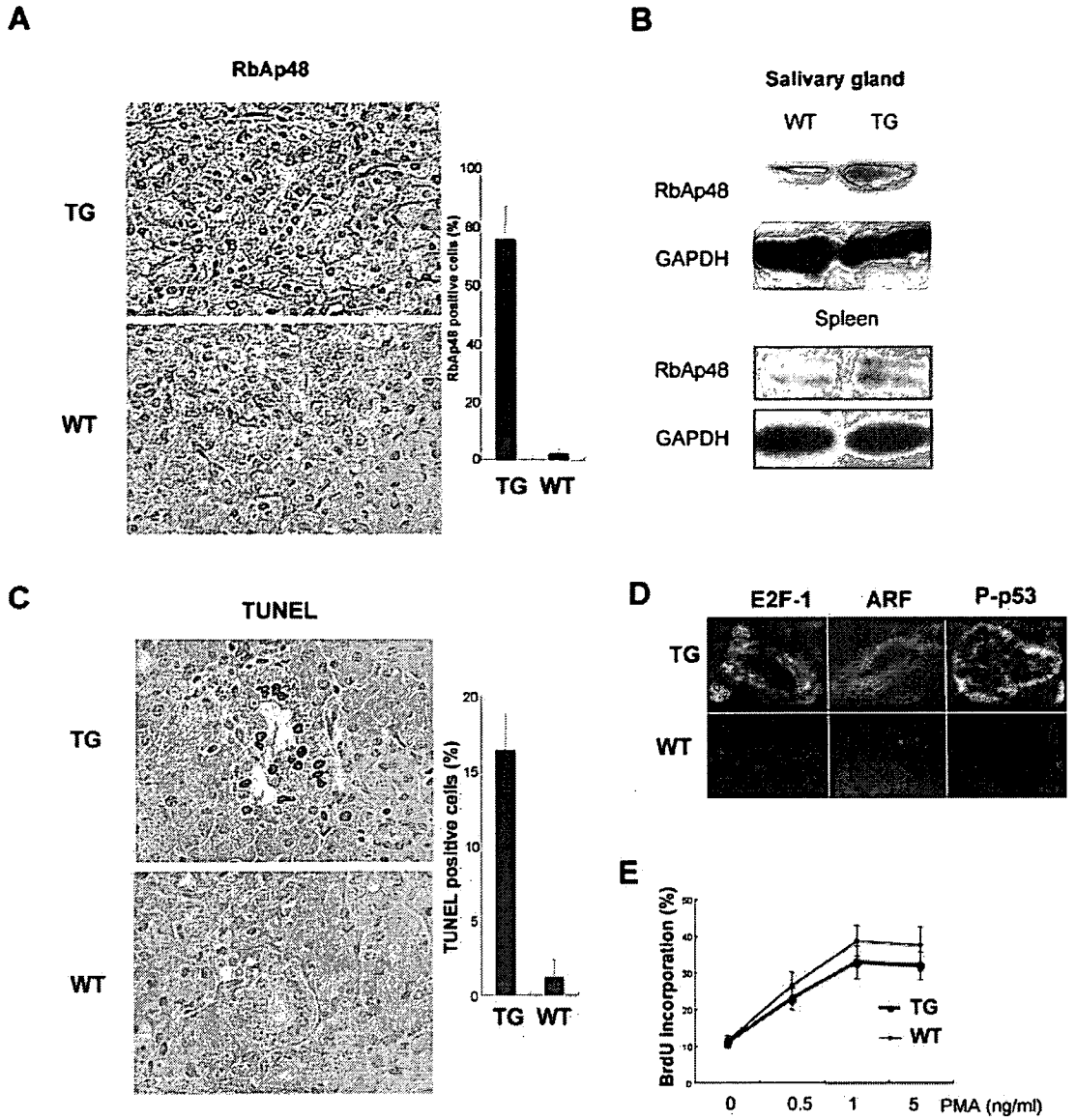

FIG. 6. RbAp48 overexpression and apoptosis in TG mice. (A) RbAp48 overexpression in the salivary gland tissues of TG mice but not WT mice at the age of 20 weeks detected by immunohistology. The percentage of RbAp48$^+$ cells was enumerated as described above (legend of Fig. 2B). (B) RbAp48 expression in the salivary gland tissues at the age of 20 weeks of TG mice compared with age-matched WT mice as detected by Western blotting. No differences in the levels of RbAp48 expression in spleens of WT and TG mice were detected. GAPDH expression was used for an internal control. (C) TUNEL$^+$ apoptotic epithelial duct cells were found in salivary glands of TG mice but not of age-matched WT mice at the age of 20 weeks. The percentage of TUNEL$^+$ cells was enumerated as described above. Images are representative of five mice. (D) Expression of E2F-1, p19ARF, and P-p53 was observed by confocal microscopy in the salivary glands of RbAp48-TG mice but not WT mice. Images are representative of five mice. (E) BrdU studies of TG mice with ectopic RbAp48 in the salivary glands demonstrated that cellular proliferation is barely affected. The graph is representative of three mice.

FIG. 5. RbAp48/E2F1/ARF-p53 pathway in the salivary glands. (A) Overexpression of RbAp48 in MSG cells from B6 mice induced E2F-1, p19ARF, and phospho-p53 (P-p53) expression, and the inhibitory effect of siRNA (15 nM) of RbAp48 was observed by confocal microscopic analysis. Cont, irrelevant siRNA control. Images are representative of three independent experiments. (B) TAM-induced apoptosis was associated with RbAp48 in MSG cells from B6 mice but not from ER$^{-/-}$, E2F1$^{-/-}$, and p53$^{-/-}$ mice as detected by confocal microscopy. Images are representative of two independent experiments. (C) Coexpression of RbAp48/E2F1, RbAp48/p19ARF, and RbAp48/p53 was detected by double-labeled confocal microscopic analysis in MSG cells of OVX B6 mice but not sham B6 mice. No differences in RbAp48/E2F1, RbAp48/p19ARF, and RbAp48/p53 expression levels were observed in MSG cells of non-OVX and OVX ER$^{-/-}$, E2F1$^{-/-}$, and p53$^{-/-}$ mice. Photos are representative of two independent experiments.

lacking many N- and C-terminal phosphorylation sites (36). These findings suggest that p53 phosphorylation is a key step in E2F-1-mediated apoptosis. The transcription factor E2F-1 functions as a key regulator for both cell cycle progression and apoptosis. E2F-2-deficient T lymphocytes exhibit enhanced T-cell receptor-stimulated proliferation and a lower activation threshold, leading to the accumulation of a population of autoreactive T lymphocytes, which appear to be responsible for causing autoimmunity in E2F-2-deficient mice (24). E2F-1$^{-/-}$ mice exhibit a defect in T lymphocyte development leading to an excess of mature T cells due to a maturation stage-specific defect in thymocyte apoptosis (8).

Our recent study suggests that antiestrogenic actions have a potent effect on the proteolysis of α-fodrin autoantigen in the salivary glands through upregulation of caspase 1 and caspase 3 activity (14). We found here a proteolysis of α-fodrin and a significant increase in caspase 3 activity in addition to the elevated caspase 1 and caspase 8 activity on RbAp48-induced apoptotic HSG cells. The fodrin α-subunit of various cells has been shown to be cleaved in association with apoptosis, in particular, due to upregulation of caspase 3 (4, 15, 48). Several reports have demonstrated that estrogen may play an inhibitory role in apoptosis in endothelial cells, breast cancer cells, cardiac myocytes, prostate cells, and neuronal cells (30, 32, 41, 43). Moreover, it has been noted that some enzymatic activities are elevated in postmenopausal women compared with normal healthy women (1, 27). Increased caspase levels seem to potentiate cell death in the presence of p53-generated signals that trigger caspase activation. Activated caspases digest many cellular proteins responsible for cell cycle regulation (e.g., Rb and Mdm2) (16), DNA damage recognition and repair [e.g., DNA-dependent protein kinase, p53, and poly(ADP-ribose) polymerase], and regulation of the cellular structure (e.g., actin, lamin, and fodrin) (44, 45). All these functional and structural protein modifications lead directly to apoptosis. Moreover, RbAp48 is found not only in histone deacetylase complexes but also in ATP-dependent remodeling complexes (9). Here we show that RbAp48 specifically activates E2F-1-mediated p53 phosphorylation in the salivary gland cells but not in many of the other types of cells examined. Thus, although the association of RbAp48 with nuclear transcriptional coactivators has not been described, there is abundant evidence that these histone binding factors interact with related classes of proteins (53, 46).

Taken together, our results demonstrate a direct molecular mechanism by which estrogen deficiency might promote p53-mediated apoptosis exclusively in exocrine gland cells through RbAp48 overexpression.

ACKNOWLEDGMENT

This work was supported in part by a Grant-in-Aid for Scientific Research (no. 17109016 and 17689049) from the Ministry of Education, Science and Culture of Japan.

REFERENCES

1. **Acarturk, F., and J. R. Robinson.** 1996. Vaginal permeability and enzymatic activity studies in normal and ovariectomized rabbits. Pharm. Res. **13**:779–783.
2. **Apostolou, I., Z. Hao, K. Rajewsky, and H. von Boehmer.** 2003. Effective destruction of Fas-deficient insulin-producing B cells in type 1 diabetes. J. Exp. Med. **198**:1103–1106.
3. **Christen, U., and M. G. Von Herrath.** 2002. Apoptosis of autoreactive CD8 lymphocytes as a potential mechanism for the abrogation of type 1 diabetes by islet-specific TNF-α expression at a time when the autoimmune process is already ongoing. Ann. N. Y. Acad. Sci. **958**:166–169.
4. **Cryns, V. L., L. Bergeron, H. Zhu, H. Li, and J. Yuan.** 1996. Specific cleavage of alpha-fodrin during Fas- and tumor necrosis factor-induced apoptosis is mediated by an interleukin-1beta-converting enzyme/Ced-3 protease distinct from the poly(ADP-ribose) polymerase protease. J. Biol. Chem. **271**:31277–31282.
5. **Ding, H. F., Y. L. Lin, G. McGill, P. Juo, H. Zhu, J. Blenis, J. Yuan, and D. E. Fisher.** 2000. Essential role for caspase-8 in transcription-independent apoptosis triggered by p53. J. Biol. Chem. **275**:38905–38911.
6. **Dou, Q. P., B. An, and P. L. Will.** 1995. Induction of a retinoblastoma phosphatase activity by anticancer drugs accompanies p53-independent G1 arrest and apoptosis. Proc. Natl. Acad. Sci. USA **92**:9019–9023.
7. **Enders, A., P. Bouillet, H. Puthalakath, Y. Xu, D. M. Tarlinton, and A. Strasser.** 2003. Loss of the proapoptotic BH3-only Bcl-2 family member Bim inhibits BCR stimulation-induced apoptosis and deletion of autoreactive B cells. J. Exp. Med. **198**:1119–1126.
8. **Field, S. J., F. Y. Tsai, F. Kuo, A. M. Zubiaga, W. G. Kaelin, Jr., D. M. Livingston, S. H. Orkin, and M. E. Greenberg.** 1996. E2F-1 functions in mice to promote apoptosis and suppress proliferation. Cell **85**:549–561.
9. **Gdula, D. A., R. Sandaltzopoulos, T. Tsukiyama, V. Ossipow, and C. Wu.** 1998. Inorganic pyrophosphatase is a component of the *Drosophila* nucleosome remodeling factor complex. Genes Dev. **12**:3206–3216.
10. **Haneji, N., T. Nakamura, K. Takio, K. Yanagi, H. Higashiyama, I. Saito, S. Noji, H. Sugino, and Y. Hayashi.** 1997. Identification of α-fodrin as a candidate autoantigen in primary Sjogren's syndrome. Science **276**:604–607.
11. **Hiebert, S. W.** 1993. Regions of the retinoblastoma gene product required for its interaction with the E2F transcription factor are necessary for E2 promoter repression and pRb-mediated growth suppression. Mol. Cell. Biol. **13**:3384–3391.
12. **Hugues, S, E. Mougneau, W. Ferlin, D. Jeske, P. Hofman, D. Homann, L. Beaudoin, C. Schrike, M. Von Herrath, A. Lehuen, and N. Glaichenhaus.** 2002. Tolerance to islet antigens and prevention from diabetes induced by limited apoptosis of pancreatic β cells. Immunity **16**:169–181.
13. **Ishimaru, N., K. Saegusa, K. Yanagi, N. Haneji, I. Saito, and Y. Hayashi.** 1999. Estrogen deficiency accelerates autoimmune exocrinopathy in murine Sjogren's syndrome through Fas-mediated apoptosis. Am. J. Pathol. **155**:173–181.
14. **Ishimaru, N., R. Arakaki, M. Watanabe, M. Kobayashi, K. Miyazaki, and Y. Hayashi.** 2003. Development of autoimmune exocrinopathy resembling Sjogren's syndrome in estrogen deficient mice of healthy background. Am. J. Pathol. **163**:1481–1490.
15. **Janicke, R. U., M. L. Sprengart, M. R. Wati, and A. G. Porter.** 1998. Caspase-3 is required for DNA fragmentation and morphological changes associated with apoptosis. J. Biol. Chem. **273**:9357–9360.
16. **Katsuda, K., M. Kataoka, F. Uno, T. Murakami, T. Kondo, J. A. Roth, N. Tanaka, and T. Fujiwara.** 2002. Activation of caspase-3 and cleavage of Rb are associated with p16-mediated apoptosis in human non-small cell lung cancer cells. Oncogene **21**:2108–2113.
17. **Kyprianou, N., H. F. English, N. E. Davidson, and J. T. Isaacs.** 1991. Programmed cell death during regression of the MCF-7 human breast cancer following estrogen ablation. Cancer Res. **51**:162–166.
18. **Lai, A., J. M. Lee, W. M. Yang, J. A. DeCaprio, W. G. Kaelin, Jr., E. Seto, and P. E. Branton.** 1999. RBP1 recruits both histone deacetylase-dependent and -independent repression activities to retinoblastoma family proteins. Mol. Cell. Biol. **19**:6632–6641.
19. **Lamhamedi-Cherradi, S. E., S. J. Zheng, K. A. Maguschak, J. Peschon, and Y. H. Chen.** 2003. Defective thymocyte apoptosis and accelerated autoimmune diseases in TRAIL$^{-/-}$ mice. Nat. Immunol. **4**:255–260.
20. **Lieman, J. H., L. A. Worley, and J. W. Harbour.** 2005. Loss of Rb-E2F repression results in caspase-8-mediated apoptosis through inactivation of focal adhesion kinase. J. Biol. Chem. **280**:10484–10490.
21. **Marchenko, N. D., A. Zaika, and U. M. Moll.** 2000. Death signal-induced localization of p53 protein to mitochondria. A potential role in apoptotic signaling. J. Biol. Chem. **275**:16202–16212.
22. **Mikkelsen, T. R., J. Brandt, H. J. Larsen, B. B. Larsen, K. Poulsen, J. Ingerslev, N. Din, and J. P. Hjorth.** 1992. Tissue-specific expression in the salivary glands of transgenic mice. Nucleic Acids Res. **20**:2249–2255.
23. **Miyagishi, M., and K. Taira.** 2002. U6 promoter-driven siRNAs with four uridine 3′ overhangs efficiently suppress targeted gene expression in mammalian cells. Nat. Biotechnol. **20**:497–500.
24. **Murga, M., O. Fernandez-Capetillo, S. J. Field, B. Moreno, L. R. Borlado, Y. Fujiwara, D. Balomenos, A. Vicario, A. C. Carrera, S. H. Orkin, M. E. Greenberg, and A. M. Zubiaga.** 2001. Mutation of E2F2 in mice causes enhanced T lymphocyte proliferation, leading to the development of autoimmunity. Immunity **15**:959–970.
25. **Nicolas, E., S. Ait-Si-Ali, and D. Trouche.** 2001. The histone deacetylase HDAC3 targets RbAp48 to the retinoblastoma protein. Nucleic Acids Res. **29**:3131–3136.
26. **Nicolas, E., V. Morales, L. Magnaghi-Jaulin, A. Harel-Bellan, H. Richard-Foy, and D. Trouche.** 2000. RbAp48 belongs to the histone deacetylase complex

that associates with the retinoblastoma protein. J. Biol. Chem. 275:9797–9804.
27. **Oner, P., S. Bekpinar, F. Cinar, and A. Argun.** 1994. Relationship of some endogenous sex steroid hormones to leukocyte arylsulphatase A activities in pre- and postmenopausal healthy women. Horm. Metab. Res. 26:301–304.
28. **Oren, M.** 2003. Decision making by p53: life, death and cancer. Cell Death Differ. 10:431–442.
29. **Paramio, J. M., C. Segrelles, M. L. Casanova, and J. L. Jorcano.** 2000. Opposite functions for E2F1 and E2F4 in human epidermal keratinocyte differentiation. J. Biol. Chem. 275:41219–41226.
30. **Pelzer, T., M. Schumann, M. Neumann, T. de Jager, M. Stimpel, E. Serfling, and L. Neyses.** 2000. 17β-Estradiol prevents programmed cell death in cardiac myocytes. Biochem. Biophys. Res. Commun. 268:192–200.
31. **Petrovsky, N., D. Silva, L. Socha, R. Slattery, and B. Charlton.** 2002. The role of Fas ligand in beta cell destruction in autoimmune diabetes of NOD mice. Ann. N. Y. Acad. Sci. 958:204–208.
32. **Pike, C. J.** 1999. Estrogen modulates neuronal Bcl-xL expression and beta-amyloid-induced apoptosis: relevance to Alzheimer's disease. J. Neurochem. 72:1552–1563.
33. **Qian, Y. W., and E. Y. Lee.** 1995. Dual retinoblastoma-binding proteins with properties related to a negative regulator of ras in yeast. J. Biol. Chem. 270:25507–25513.
34. **Qian, Y. W., Y. C. Wang, R. E. Jr. Hollingsworth, D. Jones, N. Ling, and E. Y. Lee.** 1993. A retinoblastoma-binding protein related to a negative regulator of Ras in yeast. Nature 364:648-652.
35. **Rathmell, J. C., and C. B. Thompson.** 2002. Pathways of apoptosis in lymphocyte development, homeostasis, and disease. Cell 109:S97–107.
36. **Rogoff, H. A., M. T. Pickering, M. E. Debatis, S. Jones, and T. F. Kowalik.** 2002. E2F1 induces phosphorylation of p53 that is coincident with p53 accumulation and apoptosis. Mol. Cell. Biol. 22:5308–5318.
37. **Ruuls, S. R., R. M. Hoek, V. N. Ngo, T. McNeil, L. A. Lucian, M. J. Janatpour, H. Korner, H. Scheerens, E. M. Hessel, J. G. Cyster, L. M. McEvoy, and J. D. Sedgwick.** 2001. Membrane-bound TNF supports secondary lymphoid organ structure but is subservient to secreted TNF in driving autoimmune inflammation. Immunity 15:533–543.
38. **Saegusa, K., N. Ishimaru, K. Yanagi, K. Mishima, R. Arakaki, T. Suda, I. Saito, and Y. Hayashi.** 2002. Prevention and induction of autoimmune exocrinopathy is dependent on pathogenic autoantigen cleavage in murine Sjogen's syndrome. J. Immunol. 169:1050–1057.
39. **Saito, I., K. Haruta, M. Shimuta, H. Inoue, H. Sakurai, K. Yamada, N. Ishimaru, H. Higashiyama, T. Sumida, H. Ishida, T. Suda, T. Noda, Y. Hayashi, and K. Tsubota.** 1999. Fas ligand-mediated exocrinopathy resembling Sjogren's syndrome in mice transgenic for IL-10. J. Immunol. 162: 2488–2494.
40. **Shirasuna, K., M. Sato, and T. Miyazaki.** 1981. A neoplastic epithelial duct cell line established form an irradiated human salivary gland. Cancer 48: 745–752.
41. **Spyridopoulos, I., A. Sullivan, M. Kearney, J. Isner, and D. Losordo.** 1997. Estrogen-receptor-mediated inhibition of human endothelial cell apoptosis. Estradiol as a survival factor. Circulation 95:1505–1514.
42. **Stassi, G., and R. De Maria.** 2002. Autoimmune thyroid disease: new models of cell death in autoimmunity. Nat. Rev. Immunol. 2:195–204.
43. **Szende, B., I. Romics, and L. Vass.** 1993. Apoptosis in prostate cancer after hormonal treatment. Lancet 342:1422.
44. **Tan, X., and J. Y. J. Wang.** 1998. The caspase-RB connection in cell death. Trends Cell Biol. 8:116–120.
45. **Vanags, D. M., M. I. Porn-Ares, S. Coppola, D. H. Burgess, and S. Orrenius.** 1996. Protease involvement in fodrin cleavage and phosphatidylserine exposure in apoptosis. J. Biol. Chem. 271:31075–31085.
46. **Vaute, O., E. Nicolas, L. Vandel, and D. Trouche.** 2002. Functional and physical interaction between the histone methyl transferase Suv39H1 and histone deacetylases. Nucleic Acids Res. 30:475–481.
47. **Vousden, K. H.** 2000. p53: death star. Cell 103:691–694.
48. **Wang, K. K., R. Posmantur, R. Nath, K. McGinnis, M. Whitton, R. V. Talanian, S. B. Glantz, and J. S. Morrow.** 1998. Simultaneous degradation of αII- and βII-spectrin by caspase 3 (CPP32) in apoptotic cells. J. Biol. Chem. 273:22490–22497.
49. **Wang, R. H., C. W. Liu, V. L. Avramis, and N. Berndt.** 2001. Protein phosphatase 1α-mediated stimulation of apoptosis is associated with dephosphorylation of the retinoblastoma protein. Oncogene 20:6111–6122.
50. **Whitacre, C. C.** 2001. Sex differences in autoimmune disease. Nat. Immunol. 2:777–780.
51. **Whitacre, C. C., S. C. Reingold, and P. A. O'Looney.** 1999. A gender gap in autoimmunity. Science 283:1277–1278.
52. **Yu, J. Y., S. L. DeRuiter, and D. L. Turner.** 2002. RNA interference by expression of short-interfering RNAs and hairpin RNAs in mammalian cells. Proc. Natl. Acad. Sci. USA 99:6047–6052.
53. **Zhang, Q., N. Vo, and R. H. Goodman.** 2000. Histone binding protein RbAp48 interacts with a complex of CREB binding protein and phosphorylated CREB. Mol. Cell. Biol. 20:4970–4978.
54. **Zhang, Y., B. O'Brien, J. Trudeau, R. Tan, P. Santamaria, and J. P. Dutz.** 2002. In situ β cell death promotes priming of diabetogenic CD8 T lymphocytes. J. Immunol. 168:1466–1472.

Original Paper

Pathobiology

Pathobiology 2006;73:261–270
DOI: 10.1159/000098212

Received: September 19, 2006
Accepted after revision: November 2, 2006

Biological and Oncogenic Properties of *p53*-Deficient Salivary Gland Epithelial Cells with Particular Emphasis on Stromal-Epithelial Interactions in Tumorigenesis

Kumi Obara[a] Fumio Ide[a] Kenji Mishima[a] Hiroko Inoue[a] Hiroyuki Yamada[a]
Yoshio Hayashi[b] Ichiro Saito[a]

[a]Department of Pathology, Tsurumi University School of Dental Medicine, Yokohama, and [b]Department of Oral Molecular Pathology, Institute of Health Biosciences, University of Tokushima Graduate School, Tokushima, Japan

Key Words
IGF-IR · Insulin-like growth factor-II · *PLAG1* · *p53*-deficient epithelial cells · Salivary gland tumorigenesis · Stromal-epithelial interaction

Abstract
Objective: To understand the salivary gland pathobiology, we established an immortalized duct/basal cell line (MSE) from the submandibular glands of *p53*-deficient mice. ***Methods:*** A variety of culture assays and xenograft experiments were conducted. Cellular characteristics were analyzed using histological, immunohistochemical, ultrastructural, and molecular techniques. ***Results:*** Inoculation of a mixture of MSE and Matrigel reconstructed polarized ducts whereas cotransplantation of MSE with both Matrigel and NIH3T3 (3T3) cells developed mixed tumors of adenoma and sarcoma. A daughter adenoma line (MSA) showed some transformed phenotype in vitro, but was marginally tumorigenic in vivo. Notably, pleomorphic adenoma gene 1 *(PLAG1)* was expressed in MSA but not in MSE. As compared with MSE, MSA showed higher levels of insulin-like growth factor-I receptor *(IGF-IR)*. Interestingly, 3T3 sarcoma secreted insulin-like growth factor-II (IGF-II), while MSA did not. ***Conclusion:*** The intrinsic tumorigenic programs of *p53* null salivary epithelium are promoted by 3T3 sarcoma-derived IGF-II in a paracrine manner through overexpression of *PLAG1* and *IGF-IR*.

Introduction

p53 is crucial in maintaining genome stability through a cell cycle control checkpoint. If *p53* ceases to function, affected cells undergo dysregulated growth and eventually result in neoplastic transformation by the consecutive acquisition of genetic/epigenetic alterations [1]. It is evident that the inherent or acquired loss of *p53* can release cell cycle restraints and endow cells in culture with a selective growth advantage, thereby leading to immortalization without entering senescence [2]. Conversely, the whole-body knockout of *p53* in mice represents a powerful means of generating immortalized epithelial clones that retain the original phenotypic and functional characteristics [3–5]. In this experiment, in order to exploit the deficiency of *p53*, we established epithelial cells from the submandibular glands of *p53* null adult mice. We found that MSE, one of the characterized established epithelial cell lines, may stem from the duct/basal unit

KARGER
Fax +41 61 306 12 34
E-Mail karger@karger.ch
www.karger.com

1015–2008/06/0735–0261$23.50/0

Accessible online at:
www.karger.com/pat

Dr. Ichiro Saito
Department of Pathology, Tsurumi University School of Dental Medicine
2-1-3, Tsurumi, Tsurumi-ku
Yokohama, 230-8501 (Japan)
Tel. +81 45 580 8360, Fax +81 45 572 2888, E-Mail saito-i@tsurumi-u.ac.jp

because of the inherent capacity to form duct structures in vitro and in vivo. Therefore, further studies in MSE might provide some insights into the mechanisms for salivary tubulogenesis [6]. Shortly after the breakthrough discovery of *p53*, it is clear that immortalization through *p53* loss is held to be a critical step in neoplastic transformation [1]. Indeed, *p53*-deficient mesenchymal cells are known to spontaneously acquire the ability to form tumors, after continuing growth in vitro [2, 7, 8]. By contrast, all epithelial cell lines established from *p53* null mice, including MSE, remain nontumorigenic at any passage [3, 9–11]. An impressive amount of information indicates that mesenchyme is not a passive structural bystander and that disruptive stresses of epithelial-mesenchymal cell and cell-extracellular matrix dialogue have profound influences on the fidelity of epithelial morphogenesis [12, 13]. Similar to organogenesis, it is a consensus of opinion that epithelial tumorigenesis requires a high degree of spatial and temporal orchestration of epithelium and its surrounding stroma [12–17]. In the case of salivary glands, evidence pointing to a significant role of stroma as a modulator of tumors is based on the historical observation that neoplastic transformation of embryonic mouse submandibular epithelium by polyoma virus was found only when cocultured with embryonic salivary mesenchyme [18]. Because of a dearth of model systems, very little is known about how stromal microecology participates in and contributes to the development of salivary gland tumors.

To dissect the fundamental pathway governing neoplastic conversion of *p53*-deficient epithelial cells, we devised MSE experiments. One of the most provocative implications is that MSE became dramatically tumorigenic, when cotransplanted with both 3T3 cells and Matrigel. Daughter line MSA purified from xenograft tumors showed overexpression of pleomorphic adenoma gene 1 *(PLAG1)* and insulin-like growth factor-I receptor *(IGF-IR)*. Given that 3T3 sarcoma (3T3T) produced sufficient levels of insulin-like growth factor-II (IGF-II), the present salivary adenoma formation may be the direct consequence of stromal-epithelial interactions via PLAG1/IGF-II signaling cascade.

Materials and Methods

Mice

Eight-week-old female *p53* null mice of a C57BL/6 background and 6- to 8-week-old female BALB/c athymic nude mice were purchased from the Jackson Laboratory (Bar Harbor, Me., USA) and Nihon CLEA (Tokyo, Japan), respectively. They were housed in a specific pathogen-free facility. All experiments were conducted with the approval of the Institutional Animal Care and Use Committee at the Tsurumi University.

Cell Lines

3T3 cells were purchased from American Type Culture Collection (Rockville, Md., USA) and a cell line of human adenoid cystic carcinoma (AdCC) was generously provided by Dr. T. Sakai (Osaka University, Osaka, Japan). Both cells were maintained in Dulbecco's modified Eagle medium (DMEM, Sigma Chemical Co., St. Louis, Mo., USA) supplemented with 10% fetal bovine serum at 37°C with 5% CO_2 atmosphere.

Establishment of New Cell Lines

Ten pieces of minced submandibular glands dissected from *p53* null mice were placed on cell culture plates coated with type I collagen (Sigma). After outgrowth, limiting dilution cloning was performed for sorting MSE. Similarly, MSA and 3T3T were also subcloned from tumors derived from xenografts of MSE, Matrigel (BD Biosciences, San Jose, Calif., USA) and 3T3. Both MSE and MSA were cultured in the keratinocyte-SFM (Invitrogen, Carlsbad, Calif., USA), with the supplement of epidermal growth factor (R&D Systems, Minneapolis, Minn., USA) and bovine pituitary extract (Invitrogen). To confirm the cell phenotype, standard immunocytochemical procedures were used.

Electron Microscopy

MSE and the MSE/Matrigel/3T3 tumor were primarily fixed in 2.5% glutaraldehyde and postfixed in 1% osmium tetroxide. Epon-embedded, ultrathin sections were stained with uranyl acetate and lead citrate, and examined in an H-7000 electron microscope (Hitachi, Tokyo, Japan).

Western Blotting

MSE, 3T3 and 3T3T were homogenized in NP-40 lysis buffer (Invitrogen). The whole cell lysates were fractionated by SDS polyacrylamide gel and transferred to PVDF membranes (Millipore, Bedford, Mass., USA). After blocking with 5% skim milk for 1 h, membranes were incubated overnight at 4°C with primary antibody against cytokeratin CK14 (GP-CK14, Progen Biotechnik, Heidelberg, Germany), CK8/18 (Progen Biotechnik), or α-smooth muscle actin (α-SMA, Progen Biotechnik) for MSE, and with antibody against IGF-II (R&D Systems) for 3T3 and 3T3T. The immunoreaction was detected by enhanced chemiluminescence (Amersham Biosciences, Arlington Heights, Ill., USA), followed by 1 h incubation with peroxidase-conjugated secondary anti-guinea pig or anti-mouse antibody (Zymed Lab., San Francisco, Calif., USA). Finally, they were developed by XAR film (Eastman Kodak, Rochester, N.Y., USA). The relative density of each band was determined with ImageJ software (http://rsb.info.nih.gov/ij).

Reverse Transcription-Polymerase Chain Reaction

Total RNA was extracted from the cells by TRIzol reagent (Invitrogen) and then treated with DNase I (Invitrogen). Using a cDNA synthesis kit (Superscript II DNA preamplification system, Invitrogen), cDNA was reverse-transcribed from 2 μg of RNA. Polymerase chain reaction (PCR) was conducted in 30 μl of reaction mixture (1× PCR buffer, ex Taq DNA polymerase, Takara Biomedicals, Kyoto, Japan). Sequences for specific primers were:

amylase, 5′-GGATGGAGAAAAGATGTCCTAC-3′ (forward) and 5′-CATCACCCGTGTGAAACC-3′ (reverse); *PLAG1*, 5′-TTTCCCTGAAGGGGC-3′ (forward) and 5′-GGTATTGTAGCTCTTGCCAC-3′ (reverse); *IGF-IR*, 5′-CAAGCTGTGTGTCTCCGAAA-3′(forward)and5′-TGATGAGATCCCGGTAGTCC-3′ (reverse), and *IGF-II*, 5′-TCAGAGAGGCCAAACGTCATC-3′ (forward) and 5′-GGTCTTTGGGTGGTAACAGCAT-3′ (reverse). Initial denature for PCR was 94°C for 2 min. Next, 30 cycles were done, each consisting of 94°C for 30 s, 58°C for 30 s and 72°C 30 s, and the final extension was 72°C for 10 min. PCR products were separated by 2% agarose gel. At least three measurements were performed for each sample.

Cell Proliferation Assay

MSE and MSA were plated at a density of 3×10^3/96-well plate and stimulated by different doses of epidermal growth factor, fibroblast growth factor-II, transforming growth factor-α, hepatocyte growth factor, or IGF-II, all purchased from R&D Systems. The growth rate was analyzed by the cell count reagent SF (Nacalai Tesque, Kyoto, Japan). The absorbance was measured on a Dynatech MR600 microplate Reader (Dynatech Lab., Chantilly, Va., CA), using a test wavelength of 450 nm and a reference wavelength of 600 nm, respectively.

In vitro Branching Assay

MSE were implanted at a density of 4×10^5 cells into Matrigel-coated 6-well plates and then maintained for 14 days without further treatment.

Xenograft Assay

Xenografts with different stromal conditions were prepared: one-way xenografts (2×10^6 MSE or 2×10^6 MSA only); two-way xenografts (2×10^6 MSE + Matrigel or 2×10^6 MSA + Matrigel), and three-way xenografts (1×10^6 MSE + Matrigel + 5×10^6 3T3 or 1×10^6 MSA + Matrigel + 5×10^5 3T3). All cells were used immediately. For each group, at least 3 mice (6 total injected sites) were used. Mice were monitored daily for 12 weeks.

The tumors which developed were measured in three dimensions with calipers and their volume (mm^3) was calculated with the formula of $V = 0.52 \times \text{length} \times \text{width} \times \text{height}$ [19]. Resected tissues and tumors were fixed in 10% phosphate-buffered formalin. Conventional paraffin sections were stained with hematoxylin and eosin (HE) for histological analysis.

Immunohistochemistry

Formalin-fixed, paraffin-embedded sections were stained by the streptavidin-biotin-peroxidase method [Dako LSAB(2) system, Dakocytomation, Glostrup, Denmark] using CK14 (Progen Biotechnik, 1:100); heat-induced antigen retrieval was performed. Appropriate positive and negative controls were run throughout. CK14-positive foci in 5 randomly selected areas of representative MSE/Matrigel/3T3 tumors from 3 mice were calculated under a light microscope.

Real-Time Reverse Transcription PCR

Real-time reverse transcription (RT)-PCR for *IGF-IR* was performed in MSE and MSA using the MX3000P system (Stratagene, La Jolla, Calif., USA). The reaction mixture consisted of 12.5 μl of real-time PCR Master Mix (Applied Biosystems, Warrington, UK) and 1.25 μl of primer with the supplement of DNase- and RNase-free H_2O. Sample DNA (2 μl) was added to this mixture. The first step of PCR amplification was 95°C for 30 s, and then 40 cycles were performed, each consisting of 95°C for 30 s, 57°C for 30 s, and 75°C for 30 s.

Colony Formation Assay

MSE and MSA were cultured at a density of 3×10^5 cells in DMEM containing 0.36% noble agar. After cultivation for 14 days, colony numbers in soft agar formed by each cell line were counted under a phase-contrast microscope (Nikon ECLIPSE TS100, Tokyo, Japan).

In vitro Invasion Assay

A cell invasion assay was performed by the Cell Invasion kit (Chemicon, Temecula, Calif., USA). According to the manufacturer's protocol, MSE, MSA and AdCC were initially seeded at a density of 2.5×10^5 cells in the upper chambers containing serum-free DMEM. Following 30 h of incubation, only cells that invaded through Matrigel-coated transwell inserts were detached and stained with calcein-AM solution. Invasion of cells was evaluated by a fluorescence plate reader using a 480/520 nm filter. Each analysis was repeated at least in triplicate for confirmation.

Statistical Analysis

Values were expressed as the mean ± SD. Comparisons between two groups were performed by Student's t test. The level of statistical significance was set at $p < 0.05$.

Results

MSE Recapitulate Differentiated Cytoprofile of Duct/Basal Units

Five epithelial clones were successfully established. Of these, MSE retained a stable phenotype even at passage 50 (data not shown). This line exhibited a uniform epithelial morphology and never showed the propensity to pile up on the monolayer culture (fig. 1a). Ultrastructurally, cell surface microvilli, intracytoplasmic tonofilament bundles, multiple tight junctions and well-developed desmosomes were found (fig. 1b). By Western blotting, these cells expressed CK14 but were negative for CK8/18 and α-SMA (fig. 1c, upper panel). There was no detectable expression of *amylase* mRNA on a plastic dish (fig. 1c, lower panel), and even when cultured in Matrigel (data not shown) MSE did not show any differentiation along with an acinar line. Except for IGF-II, all growth factors tested dose-dependently enhanced MSE growth in varying degrees (data not shown). When implanted in Matrigel, MSE clusters elongated and budded, displaying a branching-like appearance reminiscent of salivary gland morphogenesis (fig. 1d). Consistent with the in vitro data, MSE/Matrigel xenografts formed polarized ducts lined by well-developed microvillar surface and

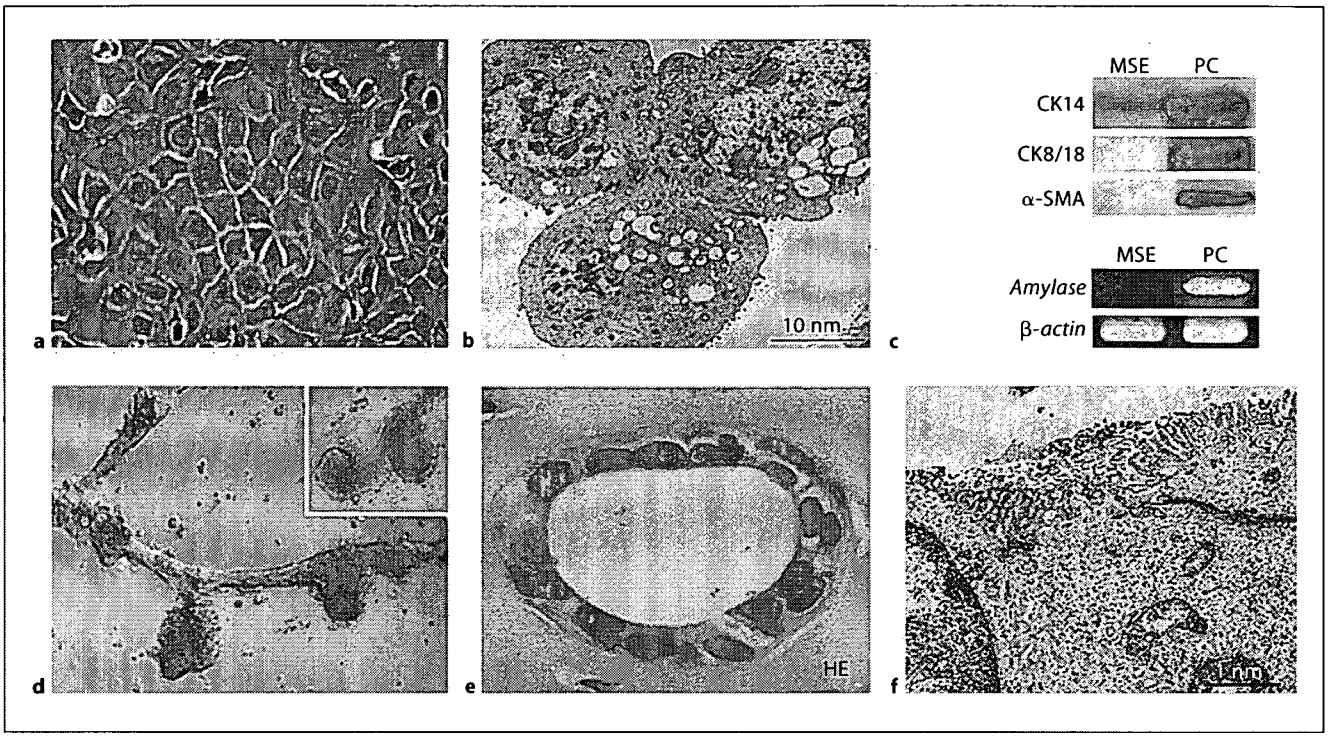

Fig. 1. Cellular profile of MSE. **a** Phase contrast at day 4 in monolayer culture showing uniform epithelial morphology. **b** Microvilli, tonofilaments and desmosomes were seen by transmission electron microscopy. **c** Western blotting showing CK14 expression (upper panel). No *amylase* mRNA was detected by RT-PCR (lower panel). PC: Whole-cell extracts from mouse submandibular glands. **d** In vitro branching 14 days after implantation in Matrigel mimicked salivary morphogenesis. Inset shows the budding formation. **e**, **f** In vivo tubulogenesis 3 months after injection with Matrigel. **e** HE histology of a well-developed duct (×400). **f** Transmission electron micrograph of duct showing long microvilli on luminal surface and multiple tight junctions.

sealed by tight junctions in vivo (fig. 1e, f). Collectively, MSE are of basal cell lineage that is programmed to differentiate into duct cells.

Sarcomatous Transformation of 3T3 Is a Key Event in MSE Tumorigenesis

All MSE/Matrigel/3T3 xenografts developed tumors within 2 weeks, while none of the others had subsequent tumors after up to 12 weeks (fig. 2a). In contrast to 3T3, mitomycin C-treated 3T3 could not foster MSE tumorigenesis. Histologically, MSE/Matrigel/3T3 tumors revealed a mixture of adenoma and sarcoma in varying proportions (fig. 2b). Adenoma components consisted of solid nests and well-formed ducts with scattered foci of squamous differentiation (fig. 2b). At the ultrastructural level, small intracellular and intercellular lumina were seen in solid tumor islands (fig. 2c). Even in multiple sections, adenoma elements lacked malignant features as compared with 3T3T. MSE tumors were immunopositive for CK14 (fig. 2d, upper panel), and the CK14-positive area percentage ranged from 15.5 to 30.3%, with a mean of 22.43% (fig. 2d, lower panel). As shown, CK14 was completely negative in nearby 3T3T cells. These in vivo results unequivocally prove that the sarcomatous change of 3T3 is critical to induce tumorigenic conversion in MSE.

MSA Exhibit Transformed Phenotypes in vitro but Are Marginally Tumorigenic in vivo

As compared with MSE, MSA showed cellular pleomorphism and several multinucleated epithelial cells were visible in the monolayer culture (fig. 3a). The proliferation rate of MSA was 2-fold higher than MSE (fig. 3b). Interestingly enough, the average number of colonies was 13 ± 2 in MSA and 1 ± 1 in MSE, showing significant difference in growth behaviors (fig. 3c). In contrast to a

MSE xenograft conditions	No. of tumors/ No. of sites injected
MSE	0/3
MSE/matrigel	0/12
MSE/matrigel/3T3	10/10
MSE/matrigel/mitomycin C-treated 3T3	0/6

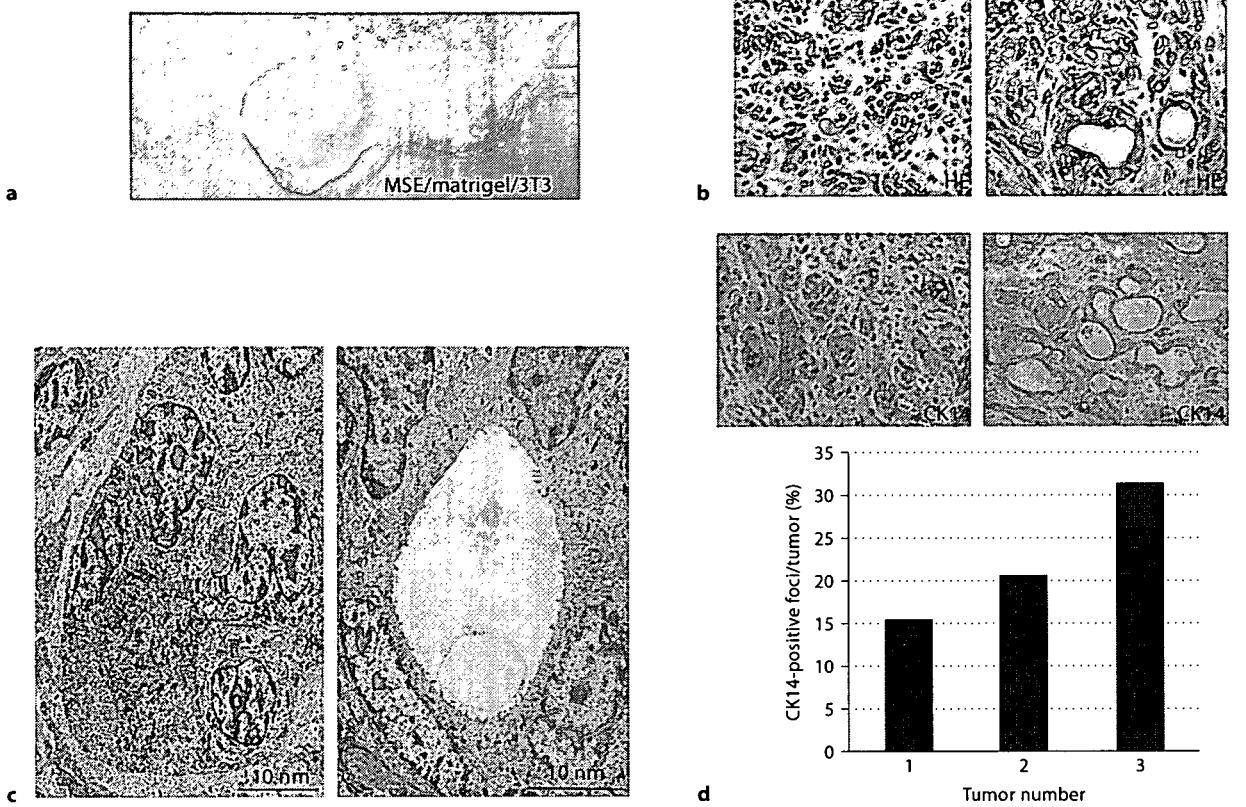

Fig. 2. Tumorigenicity assay of MSE. **a** Only MSE/Matrigel/3T3 xenografts grew as tumors visible by the naked eye. **b** HE histology of MSE/Matrigel/3T3 tumor showing solid nests (left panel; ×200) and ducts (right panel; ×200) in sarcoma. Inset shows squamous differentiation (×400). **c** Transmission electron micrograph of a solid nest (left panel) and well-formed duct (right panel). **d** Immunoexpression of CK14 in solid nests (upper left panel; ×200) and ducts (upper right panel; ×200). Approximately 22% of tumor areas were CK14-expressing adenomas (lower panel).

highly invasive AdCC, both cell lines, however, lacked invasive capacity (fig. 3d). By in vivo xenograft assay, tumors began to appear in MSA/Matrigel recombinants 4 weeks after inoculation (fig. 4a), but their size remained unchanged after up to 12 weeks (data not shown). Indeed, the volume of MSA/Matrigel tumors was far smaller than that of the MSE/Matrigel/3T3 or MSA/Matrigel/3T3 tumors. Among the three-way xenografts, MSA showed a slight increase in the tumor volume, although statistically not significant. Histologically, MSA/Matrigel tumors were compatible with ductal adenomas containing scattered squamoid foci (fig. 4b) and essentially similar to adenoma components of MSE/Matrigel/3T3 tumors (fig. 2b) and MSA/Matrigel/3T3 tumors (data not shown). Over-

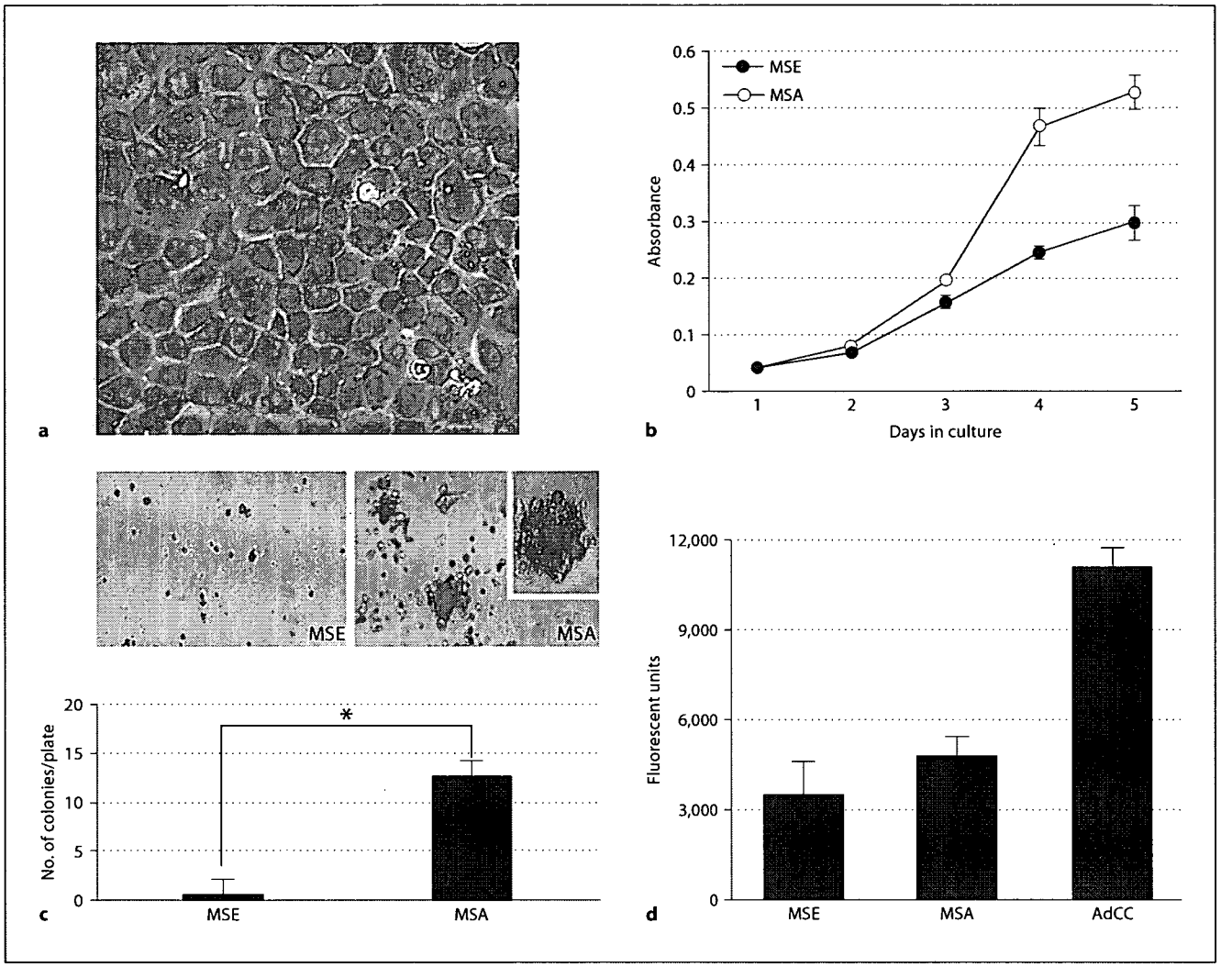

Fig. 3. Cellular profile of MSA. **a** Phase contrast at day 3 in culture showing marked morphological alteration compared to MSE (fig. 1a). **b** The growth rate of MSA was nearly 2-fold greater than that of MSA by cell proliferation assay. **c** Colony formation assay showing large MSA colonies (upper panel). Inset shows magnified colony (×400). As compared to MSE, MSA formed a significantly larger number of colonies (1 vs. 13) (lower panel). * $p < 0.05$. **d** No significant difference in invasive ability between MSE and MSA by invasion assay.

all, MSA gained some transformed phenotypes in vitro, but apparently lacked malignant properties in vivo.

Stromal-Epithelial Interactions Direct MSE Tumorigenesis through PLAG1/IGF-II Pathway

There is ongoing concern that *PLAG1* plays an important role in the development of salivary pleomorphic adenomas [20–26]. In this context, we investigated the possible involvement of *PLAG1* and its related genes in MSE tumorigenesis. As expected, *PLAG1* was evident in MSA and 3T3T, but not in MSE and 3T3 (fig. 5a). All cell lines tested expressed *IGF-IR*, with a higher expression level (>3-fold) in MSA than MSE (fig. 5a, b). On the other hand, clearly enhanced expression of IGF-II protein (>1.8-fold), a genuine target gene of *PLAG1* [22, 23], was found in 3T3T as compared with 3T3 (fig. 5c). Moreover, exposure to IGF-II accelerated the growth of MSA in a dose-dependent manner (fig. 5d). Analysis of molecular profile provides evidence that 3T3T-derived IGF-II upregulate proliferation of *PLAG1*- and *IGF-IR*-expressing

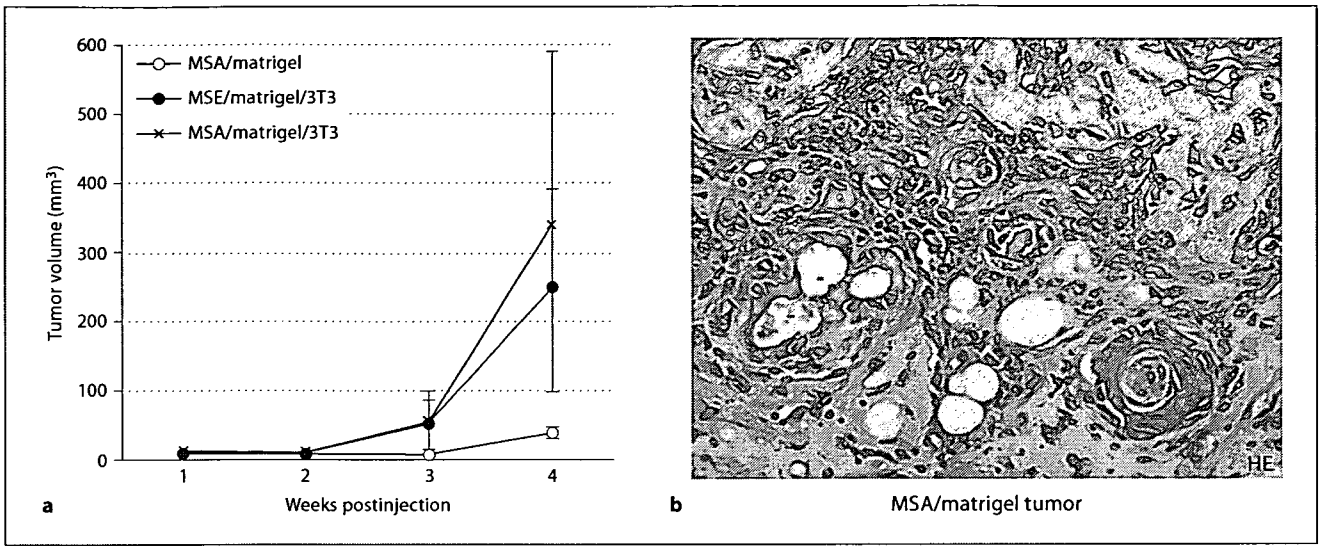

Fig. 4. Tumorigenicity assay of MSA. **a** MSA/Matrigel tumors remained small compared to MSE/Matrigel/3T3 and MSA/Matrigel/3T3 tumors. **b** HE histology of MSA/Matrigel tumor showing ductal adenoma with squamous differentiation (×200).

MSA in a paracrine manner and suggests that *PLAG1* is a possible candidate to trigger the molecular switch of preneoplastic MSE to neoplastic MSA.

Discussion

A growing body of work shows that fibroblasts function as a landscaper in the stroma [12–17, 27–30]. There have been hundreds of in vitro and in vivo tissue recombinant studies using a wide variety of epithelial and fibroblastic cells in different stages of transformation [31–34]. A key point to consider is the great deal of fibroblast heterogeneity and plasticity [14–16, 27–30]. The origin and nature such as murine versus human [35, 36], young versus old [37, 38], orthotopic versus ectopic [39, 40], and normal versus irradiated [10, 41], all intervene. In this context, we focused on the previous data using the well-defined and most prevalent 3T3 as a stromal partner for comparison. In essence, 3T3 encouraged normal and malignant human prostate epithelial cells to proliferate [42]. In human prostate cancer PC-3, original, *neu*-transfected and irradiated 3T3 cells all acted in a cooperative way to facilitate tumor formation [43]. A similar in vivo tumor-promoting effect was observed in human bladder carcinoma cells [44]. On the other hand, cotransplantation of 3T3 with another human prostate cancer line, LNCaP, failed to cause carcinoma [45]. It is also important to keep in mind that the tumor-forming potential of preneoplastic murine 3T3 [46] and marginally tumorigenic human PC-3 and LNCaP [47] is largely different in the presence or absence of a reconstituted basement membrane, Matrigel [48]. Matrigel/3T3-dependent progression of LNCaP was successfully demonstrated in the recent xenograft experiment [49]. In our working model, fibroblastic microenvironments potently tune the neoplastic conversion of MSE into MSE/Matrigel/3T3 recombinants. Although the exact molecular mechanism of 3T3 sarcomagenesis remains to be determined, a hepatocyte growth factor/c-Met autocrine axis is one of the attractive candidates [50]. On the other hand, MSE could not react to insufficient stromagenesis by growth-arrested 3T3. In the absence of Matrigel, MSE/3T3 transplants remained nontumorigenic (unpubl. data). Surprisingly, neither MSE nor MSA components could be detected in MSE/Matrigel/3T3T and MSA/Matrigel/3T3T tumors (unpubl. data), suggesting that 3T3T are not an active stromal partner. Based on our unpublished stepwise monitoring that MSE and MSA throve until 4 weeks after inoculation but eventually disappeared, it is likely that epithelial elements were gradually replaced by the vigorously growing 3T3T.

There are a few experiments in which the addition of an active oncogene *ras* or *neu* can drive neoplastic potential of *p53* null epithelial cells [3, 51–53]. Although we did

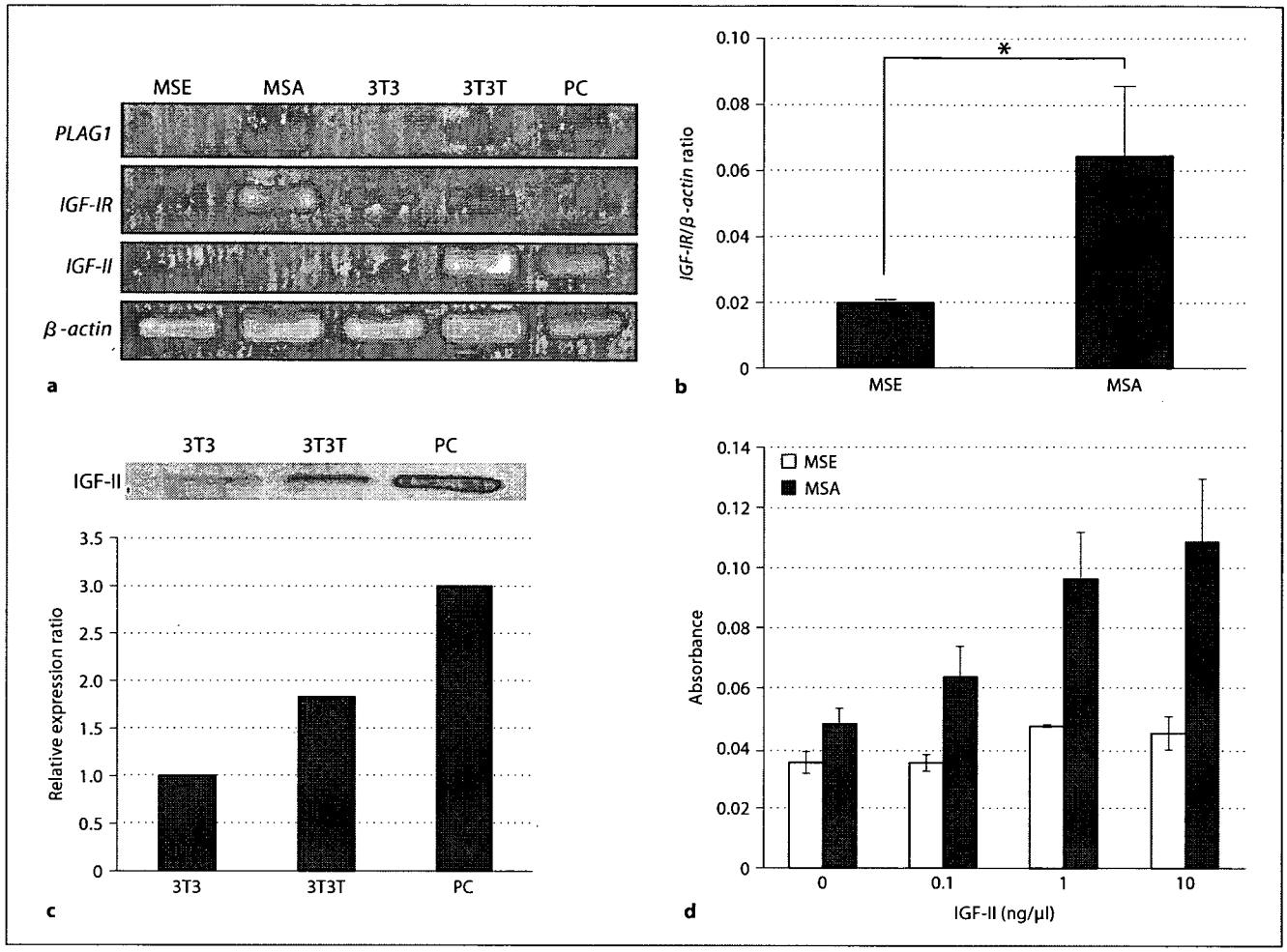

Fig. 5. Molecular mechanism of MSE tumorigenesis. **a** RT-PCR showing overexpression of *PLAG1* in MSA and 3T3T. *IGF-IR* was highly expressed in MSA, and *IGF-II* was detectable only in stromal cells. PC: Mouse brain. **b** Real-time RT-PCR demonstrated that MSA arranged >3-fold increase in *IGF-IR* expression relative to MSE. *$p < 0.05$. **c** Western blotting showing a higher level of IGF-II in 3T3T. PC: Mouse recombinant IGF-II. **d** A dose-dependent enhancement of IGF-II-inducible growth was evident in MSA by cell proliferation assay.

not introduce any exogenous genomic insult, the possibility that *p53*-deficient MSE poses unstable chromosomes (>80% of cells were aneuploid; unpubl. data), which render cells spontaneous accumulation of successive genetic changes through time, should also be considered [54]. In recent years, the contribution of the proto-oncogene *PLAG1* to salivary gland tumorigenesis has begun to emerge [20–26]. In our model, ectopic expression of *PLAG1* was evident in MSA and 3T3T. A genuine target gene of *PLAG1* is *IGF-II* and the oncogenic capacity of *PLAG1* is mediated by activating the IGF-II mitogenic pathway [22–26]. Compared with the culture supernatant of 3T3, that of 3T3T enhanced the growth of MSA in a dose-dependent manner and this was partially inhibited in the presence of the neutralizing antibody against IGF-II (data not shown). It is of note that IGF-II was produced by 3T3T, whereas it was not detectable in MSA. On the other hand, the activity of IGF-II mitogenic signaling is mainly regulated by *IGF-IR*. In fact, *IGF-IR*-deficient cells overexpressing *PLAG1* could not respond to IGF-II [23]. As shown, *IGF-IR* was highly expressed in MSA. Collectively, in contrast to an autocrine mechanism of *PLAG1*-expressing 3T3 sarcomagenesis [23], tumorigenic conversion of MSE is directed by stroma-derived IGF-II

in a paracrine manner through overexpression of *PLAG1* and *IGF-IR*. Although extensive efforts have been made, MSA/Matrigel tumors failed to grow continuously and remained small. Conversely, this phenomenon firmly establishes that *PLAG1* by itself is a benign oncogene [20–26] and also supports the notion that other than duct cells, myoepithelium significantly contributes to the formation of *PLAG1*-induced salivary gland tumors [25, 26]. Further experiments are currently underway in our laboratory to identify other *PLAG1* target genes potentially involved in MSA tumor progression.

In summary, the present results indicate that the inherent genomic instability of MSE through *p53* loss makes its phenotype very plastic, which alters under continuous stromal pressure. Our data also convincingly support the fact that *PLAG1* is a key determinant in the neoplastic transformation of salivary epithelium [20–26]. While much work remains to be done, *p53* null epithelial cells now established open a unique opportunity to probe synergistic interactions between intrinsic *PLAG1* in the epithelium and extrinsic growth signals such as IGF-II from the stroma in salivary gland tumorigenesis.

Acknowledgements

The authors gratefully thank Judith Nishino for helpful discussions during the preparation of this manuscript. This work was supported by a grant from the Smoking Research Foundation to F.I., Grants-in-Aid for Scientific Research from the Ministry of Education, Culture, Sports, Science and Technology of Japan to I.S., and Grants-in-Aid for Scientific Research from the Ministry of Health, Labor and Welfare to I.S.

References

1 Lowe SW, Cepero E, Evan G: Intrinsic tumour suppression. Nature 2004;432:307–315.

2 Harvey M, Sands AT, Weiss RS, Hegi ME, Wiseman RW, Pantazis P, Giovanella BC, Tainsky MA, Bradley A, Donehower LA: In vitro growth characteristics of embryo fibroblasts isolated from p53-deficient mice. Oncogene 1993;8:2457–2467.

3 Sevignani C, Wlodarski P, Kirillova J, Mercer WE, Danielson KG, Iozzo RV, Calabretta B: Tumorigenic conversion of p53-deficient colon epithelial cells by an activated Ki-ras gene. J Clin Invest 1998;101:1572–1580.

4 Hanazono M, Nozawa R, Itakura R, Aizawa S, Tomooka Y: Establishment of an androgen-responsive prostatic cell line 'PEA5' from a p53-deficient mouse. Prostate 2001; 46:214–225.

5 Dumble ML, Croager EJ, Yeoh GC, Quail EA: Generation and characterization of p53 null transformed hepatic progenitor cells: oval cells give rise to hepatocellular carcinoma. Carcinogenesis 2002;23:435–445.

6 Debnath J, Brugge JS: Modelling glandular epithelial cancers in three-dimensional cultures. Nat Rev Cancer 2005;5:675–688.

7 Yahanda AM, Bruner JM, Donehower LA, Morrison RS: Astrocytes derived from p53-deficient mice provide a multistep in vitro model for development of malignant gliomas. Mol Cell Biol 1995;15:4249–4259.

▶8 Bogler O, Nagane M, Gillis J, Huang HJ, Cavenee WK: Malignant transformation of p53-deficient astrocytes is modulated by environmental cues in vitro. Cell Growth Differ 1999;10:73–86.

9 Skobe M, Fusenig NE: Tumorigenic conversion of immortal human keratinocytes through stromal cell activation. Proc Natl Acad Sci USA 1998;95:1050–1055.

10 Barcellos-Hoff MH, Ravani SA: Irradiated mammary gland stroma promotes the expression of tumorigenic potential by unirradiated epithelial cells. Cancer Res 2000;60: 1254–1260.

11 Medina D, Kittrell FS, Shepard A, Stephens LC, Jiang C, Lu J, Allred DC, McCarthy M, Ullrich RL: Biological and genetic properties of the p53 null preneoplastic mammary epithelium. FASEB J 2002;16:881–883.

12 Bissell MJ, Radisky D: Putting tumours in context. Nat Rev Cancer 2001;1:46–54.

13 Liotta LA, Kohn EC: The microenvironment of the tumour-host interface. Nature 2001; 411:375–379.

14 Tlsty TD, Hein PW: Know thy neighbor: stromal cells can contribute oncogenic signals. Curr Opin Genet Dev 2001;11:54–59.

15 Cunha GR, Matrisian LM: It's not my fault, blame it on my microenvironment. Differentiation 2002;70:469–472.

16 Mueller MM, Fusenig NE: Friends or foes – bipolar effects of the tumour stroma in cancer. Nat Rev Cancer 2004;4:839–849.

17 Weaver VM, Gilbert P: Watch thy neighbor: cancer is a communal affair. J Cell Sci 2004; 117:1287–1290.

18 Dawe CJ: Epithelial-Mesenchymal Interactions in Relation to the Genesis of Polyoma Virus-Induced Tumors of Mouse Salivary Gland. London, Academic Press, 1972.

19 Janik P, Briand P, Hartmann NR: The effect of estrone-progesterone treatment on cell proliferation kinetics of hormone-dependent GR mouse mammary tumors. Cancer Res 1975;35:3698–3704.

20 Kas K, Voz ML, Roijer E, Astrom AK, Meyen E, Stenman G, Van de Ven WJ: Promoter swapping between the genes for a novel zinc finger protein and beta-catenin in pleiomorphic adenomas with t(3;8)(p21;q12) translocations. Nat Genet 1997;15:170–174.

21 Voz ML, Astrom AK, Kas K, Mark J, Stenman G, Van de Ven WJ: The recurrent translocation t(5;8)(p13;q12) in pleomorphic adenomas results in upregulation of PLAG1 gene expression under control of the LIFR promoter. Oncogene 1998;16:1409–1416.

22 Voz ML, Agten NS, Van de Ven WJ, Kas K: PLAG1, the main translocation target in pleomorphic adenoma of the salivary glands, is a positive regulator of IGF-II. Cancer Res 2000;60:106–113.

23 Hensen K, Van Valckenborgh IC, Kas K, Van de Ven WJ, Voz ML: The tumorigenic diversity of the three PLAG family members is associated with different DNA binding capacities. Cancer Res 2002;62:1510–1517.

24 Voz ML, Mathys J, Hensen K, Pendeville H, Van Valckenborgh I, Van Huffel C, Chavez M, Van Damme B, De Moor B, Moreau Y, Van de Ven WJ: Microarray screening for target genes of the proto-oncogene PLAG1. Oncogene 2004;23:179–191.

25 Declercq J, Van Dyck F, Braem CV, Van Valckenborgh IC, Voz M, Wassef M, Schoonjans L, Van Damme B, Fiette L, Van de Ven WJ: Salivary gland tumors in transgenic mice with targeted PLAG1 proto-oncogene overexpression. Cancer Res 2005;65: 4544–4553.

26 Zhao X, Ren W, Yang W, Wang Y, Kong H, Wang L, Yan L, Xu G, Fei J, Fu J, Zhang C, Wang Z: Wnt pathway is involved in pleomorphic adenomas induced by overexpression of PLAG1 in transgenic mice. Int J Cancer 2006;118:643–648.

27 Silzle T, Randolph GJ, Kreutz M, Kunz-Schughart LA: The fibroblast: sentinel cell and local immune modulator in tumor tissue. Int J Cancer 2004;108:173–180.

28 Bhowmick NA, Neilson EG, Moses HL: Stromal fibroblasts in cancer initiation and progression. Nature 2004;432:332–337.

29 Beacham DA, Cukierman E: Stromagenesis: the changing face of fibroblastic microenvironments during tumor progression. Semin Cancer Biol 2005;15:329–341.

30 Kalluri R, Zeisberg M: Fibroblasts in cancer. Nat Rev Cancer 2006;6:392–401.

31 Olumi AF, Grossfeld GD, Hayward SW, Carroll PR, Tlsty TD, Cunha GR: Carcinoma-associated fibroblasts direct tumor progression of initiated human prostatic epithelium. Cancer Res 1999;59:5002–5011.

32 Cunha GR, Hayward SW, Wang YZ, Ricke WA: Role of the stromal microenvironment in carcinogenesis of the prostate. Int J Cancer 2003;107:1–10.

33 Cornil I, Theodorescu D, Man S, Herlyn M, Jambrosic J, Kerbel RS: Fibroblast cell interactions with human melanoma cells affect tumor cell growth as a function of tumor progression. Proc Natl Acad Sci USA 1991; 88:6028–6032.

34 Chung LW, Chang SM, Bell C, Zhau HE, Ro JY, von Eschenbach AC: Co-inoculation of tumorigenic rat prostate mesenchymal cells with non-tumorigenic epithelial cells results in the development of carcinosarcoma in syngeneic and athymic animals. Int J Cancer 1989;43:1179–1187.

35 Gartner MF, Wilson EL, Dowdle EB: Fibroblast-dependent tumorigenicity of melanoma xenografts in athymic mice. Int J Cancer 1992;51:788–791.

36 Kuperwasser C, Chavarria T, Wu M, Magrane G, Gray JW, Carey L, Richardson A, Weinberg RA: Reconstruction of functionally normal and malignant human breast tissues in mice. Proc Natl Acad Sci USA 2004; 101:4966–4971.

37 Campisi J: Senescent cells, tumor suppression, and organismal aging: good citizens, bad neighbors. Cell 2005;120:513–522.

38 Maffini MV, Calabro JM, Soto AM, Sonnenschein C: Stromal regulation of neoplastic development: age-dependent normalization of neoplastic mammary cells by mammary stroma. Am J Pathol 2005;167:1405–1410.

39 Mukaida H, Hirabayashi N, Hirai T, Iwata T, Saeki S, Toge T: Significance of freshly cultured fibroblasts from different tissues in promoting cancer cell growth. Int J Cancer 1991;48:423–427.

40 Fabra A, Nakajima M, Bucana CD, Fidler IJ: Modulation of the invasive phenotype of human colon carcinoma cells by organ specific fibroblasts of nude mice. Differentiation 1992;52:101–110.

41 Ohuchida K, Mizumoto K, Murakami M, Qian LW, Sato N, Nagai E, Matsumoto K, Nakamura T, Tanaka M: Radiation to stromal fibroblasts increases invasiveness of pancreatic cancer cells through tumor-stromal interactions. Cancer Res 2004;64:3215–3222.

▶42 Kabalin JN, Peehl DM, Stamey TA: Clonal growth of human prostatic epithelial cells is stimulated by fibroblasts. Prostate 1989;14: 251–263.

▶43 Camps JL, Chang SM, Hsu TC, Freeman MR, Hong SJ, Zhau HE, von Eschenbach AC, Chung LW: Fibroblast-mediated acceleration of human epithelial tumor growth in vivo. Proc Natl Acad Sci USA 1990;87:75–79.

▶44 Zhau HE, Hong SJ, Chung LW: A fetal rat urogenital sinus mesenchymal cell line (rUGM): accelerated growth and conferral of androgen-induced growth responsiveness upon a human bladder cancer epithelial cell line in vivo. Int J Cancer 1994;56:706–714.

▶45 Gleave M, Hsieh JT, Gao CA, von Eschenbach AC, Chung LW: Acceleration of human prostate cancer growth in vivo by factors produced by prostate and bone fibroblasts. Cancer Res 1991;51:3753–3761.

▶46 Fridman R, Sweeney TM, Zain M, Martin GR, Kleinman HK: Malignant transformation of NIH-3T3 cells after subcutaneous coinjection with a reconstituted basement membrane (matrigel). Int J Cancer 1992;51: 740–744.

▶47 Passaniti A, Isaacs JT, Haney JA, Adler SW, Cujdik TJ, Long PV, Kleinman HK: Stimulation of human prostatic carcinoma tumor growth in athymic mice and control of migration in culture by extracellular matrix. Int J Cancer 1992;51:318–324.

▶48 Kleinman HK, Martin GR: Matrigel: basement membrane matrix with biological activity. Semin Cancer Biol 2005;15:378–386.

▶49 Tuxhorn JA, McAlhany SJ, Dang TD, Ayala GE, Rowley DR: Stromal cells promote angiogenesis and growth of human prostate tumors in a differential reactive stroma (DRS) xenograft model. Cancer Res 2002;62:3298–3307.

50 Cortner J, Van de GF, Rong S: The Met-HGF/SF autocrine signaling mechanism is involved in sarcomagenesis; in Goldberg ID, Rosen EM (eds): Epithelial-Mesenchymal Interactions in Cancer. Basel, Birkhäuser, 1995, pp 89–120.

▶51 Hundley JE, Koester SK, Troyer DA, Hilsenbeck SG, Subler MA, Windle JJ: Increased tumor proliferation and genomic instability without decreased apoptosis in MMTV-ras mice deficient in p53. Mol Cell Biol 1997;17: 723–731.

▶52 Brodie SG, Xu X, Li C, Kuo A, Leder P, Deng CX: Inactivation of p53 tumor suppressor gene acts synergistically with c-neu oncogene in salivary gland tumorigenesis. Oncogene 2001;20:1445–1454.

▶53 Gao J, Huang HY, Pak J, Cheng J, Zhang ZT, Shapiro E, Pellicer A, Sun TT, Wu XR: p53 deficiency provokes urothelial proliferation and synergizes with activated Ha-ras in promoting urothelial tumorigenesis. Oncogene 2004;23:687–696.

▶54 Rajagopalan H, Lengauer C: Aneuploidy and cancer. Nature 2004;432:338–341.

Original Paper

Pathobiology

Pathobiology 2006;73:252–260
DOI: 10.1159/000098211

Received: September 12, 2006
Accepted after revision: October 17, 2006

Possible Involvement of Oxidative Stress in Salivary Gland of Patients with Sjögren's Syndrome

Koufuchi Ryo[a, b] Hiroyuki Yamada[a] Yoichi Nakagawa[c] Yoshinori Tai[b]
Kumi Obara[a] Hiroko Inoue[a] Kenji Mishima[a] Ichiro Saito[a]

Departments of [a]Pathology and [b]Geriatric Dentistry, and [c]Second Department of Oral and Maxillofacial Surgery, Tsurumi University School of Dental Medicine, Yokohama, Japan

Key Words
Autoimmunity · Oxidative stress · Salivary gland · Saliva

Abstract
Objective: To determine the involvement of oxidative stress in the salivary gland of patients with Sjögren's syndrome (SS). ***Methods:*** Oxidative damage to the gland was measured by 8-hydroxy-2'-deoxyguanosine (8-OHdG) and hexanoyl-lysine (HEL) using the SS saliva. In addition, lactate dehydrogenase (LDH) and mitochondrial glutamic-oxaloacetic transaminase (m-GOT), both general markers for cell damage, were also analyzed. ***Results:*** Increased levels of 8-OHdG and HEL were found in the saliva of SS patients, but not in that of patients with other salivary gland dysfunction or of healthy individuals. Levels of LDH and m-GOT were significantly correlated with 8-OHdG and HEL levels, respectively. Furthermore, the increased levels of 8-OHdG and HEL were also correlated in the SS saliva. ***Conclusion:*** These findings suggested the involvement of oxidative stress in glandular tissue destruction in SS. It was indicated that the detection of 8-OHdG and HEL in the saliva may become a useful tool for the diagnosis of SS.

Introduction

Sjögren's syndrome (SS) is an autoimmune disease which progressively destroys the salivary and lacrimal glands, leading to the distressing symptoms of dry mouth and dry eyes [1]. The etiology of SS is obscure, with evidence implicating both environmental factors, in particular viruses, and genetic predisposition [2–4].

Oxidative stress by reactive oxygen species (ROS) is thought to participate in a wide variety of cellular functions including apoptosis [5, 6]. Several observations have suggested that ROS might mediate apopotosis: various cytotoxic stresses are sometimes accompanied by increases in intracellular ROS levels; depletion or oxidation of cellular antioxidants such as redox enzymes including thioredoxin induce apoptosis [7, 8], and many antioxidants and free radical scavengers have been shown to inhibit or delay certain types of cell death [9, 10]. There are many reports on the possible mechanism by which various pathophysiological phenomena in autoimmune diseases develop through these processes [11, 12]. Increased levels of markers for oxidative stress are found in the synovial fluid [13, 14], serum [15–17] and urine of patients with rheumatoid arthritis [18] and type I diabetes mellitus [19, 20]. However, there is a paucity of studies specifically on SS.

KARGER
Fax +41 61 306 12 34
E-Mail karger@karger.ch
www.karger.com

1015–2008/06/0735–0252$23.50/0

Accessible online at:
www.karger.com/pat

Dr. Ichiro Saito
Department of Pathology, Tsurumi University School of Dental Medicine
2-1-3 Tsurumi, Tsurumi-ku
Yokohama, 230-8501 (Japan)
Tel. +81 45 580 8360, Fax +81 45 572 2888, E-Mail saito-i@tsurumi-u.ac.jp

Table 1. Characteristics of the subjects in this study

	SS (n = 8)	G1 (non-SS) (n = 9)	G2 (non-SS) (n = 10)	Control (n = 10)
Age, years	64.6 ± 11.3	61.7 ± 11.9	68.2 ± 6.7	59.8 ± 6.5
Unstimulated saliva flow rates, ml/15 min	0.1 ± 0.1	0.3 ± 0.2	1.0 ± 0.3	3.0 ± 1.6
Stimulated saliva flow rates, ml/10 min	3.7 ± 0.5	4.1 ± 0.5	7.3 ± 1.5	15.5 ± 3.7

Values represent mean ± SD.

We have already reported on the relationship between a marked expression of thioredoxin and Epstein-Barr virus (EBV) reactivation in the salivary gland of SS patients [21]. Furthermore, our previous studies showed an increase in the enzymatic activity of apoptotic protease by EBV activation to be involved in the progression of 120-kDa α-fodrin autoantigen proteolysis during the development of SS [22, 23].

8-Hydroxy-2′-deoxyguanosine (8-OHdG) is formed when the guanine in DNA undergoes oxidative damage by ROS [24, 25]. During the process of DNA repair, 8-OHdG is released into the extracellular space [26]. By detecting this, it is possible to prove cytotoxicity via oxidative stress; thus 8-OHdG has been used widely as a useful biomarker [27–30]. The formation of hexanoyl-lysine (HEL) in lipid hydroperoxide-modified proteins including oxidatively modified low-density lipoprotein was reported as an initial marker for the oxidative damage of biological molecules in vivo [31]. The purpose of this study, therefore, is to clarify the relationship of oxidative stress to the extent of damage to the glandular tissue that is caused by such stress.

Materials and Methods

Patients and Controls

All patients were seen at the outpatient clinic of the Tsurumi University School of Dental Medicine. They all had the typical symptoms of dry mouth such as difficulty in swallowing, impaired sense of taste, or burning sensation of the tongue, each of which can be relieved by applying artificial saliva. The participants were women, and their mean age was 63.9 ± 9.6 years (range 36–86 years). Informed consent was obtained from all study subjects. Patients with unstimulated salivary test result values of <1.5 ml/15 min, and stimulated values of <10 ml/10 min were diagnosed with dry mouth, whereas patients with values of ≥10 ml were excluded from this study, despite subjective symptoms otherwise suggestive of dry mouth. The diagnosis of SS was based on the criteria proposed by Fox and Saito [32]: (1) the presence of keratoconjunctivitis sicca, where the tear volume was measured by the Schirmer I test (<5 mm/5 min), (2) dry mouth, (3) extensive lymphocytic infiltrate on minor salivary gland biopsy, and (4) laboratory evidence of a systemic autoimmune disease, which includes positive rheumatoid factor (titer ≥1:160), positive antinuclear antibodies (titer ≥1:160), or positive SS-A or SS-B antibodies. When the patients met at least three of the above criteria, they were diagnosed as having SS. These patients had not received glucocorticoids or immunosuppressive agents for at least 6 months prior to this examination. They were then divided into three different subgroups: SS group with unstimulated values of <0.5 ml/15 min and stimulated values of <5 ml/10 min; group 1 (G1): non-SS with unstimulated values of <0.5 ml/15 min and stimulated values of <5 ml/10 min, and group 2 (G2): non-SS with unstimulated values of ≥0.5 to <1.5 ml/15 min and stimulated values of ≥5 to <10 ml/10 min.

Of the 27 patients with dry mouth, 8 were classified as SS, 9 as G1 and 10 as G2. Ten normal healthy individuals served as age- and sex-matched controls with unstimulated values of ≥1.5 ml/15 min and stimulated values of ≥10 ml/10 min. The values of unstimulated and stimulated saliva flow rate in each group are shown in table 1.

Unstimulated and stimulated whole saliva was collected in the outpatient clinic between 2:00 and 4:00 p.m. to minimize the effects of diurnal variation, and the patients and healthy volunteers were instructed to avoid food or drink and smoking for at least 1 h preceding the test. Before the collection of saliva, the participants were seated in a chair and left to relax for 5 min. With the head bent forward, they then let saliva drip into a paper cup for 15 min. Thereafter, the secretion of saliva was stimulated by chewing on a piece of gum for 10 min and the stimulated saliva was collected for 10 min as described above. As the unstimulated saliva was low in volume and not a sufficient amount for testing, we used the stimulated saliva for the experiments.

Preparation of Saliva and Sera Samples

Stimulated whole saliva samples were centrifuged at 12,000 rpm for 45 min and filtered through a 0.22-μm filter to remove cells, virus and particulate debris. The blood samples were centrifuged at 3,000 rpm for 5 min and the sera separated. All saliva and sera were stored at –80°C until analysis.

Determination of Salivary and Serum 8-OHdG

Saliva and sera samples were centrifuged at 10,000 rpm for 30 min and filtration of the supernatant using an ultrafilter (cut-off molecular weight 10 kDa) was performed to exclude interfering substances. Competitive enzyme-linked immunosorbent as-

say (ELISA) [33] was conducted in triplicate using an 8-OHdG monoclonal antibody (N45.1; Institute for the Control of Aging, Shizuoka, Japan). A 50-μl aliquot of the saliva or sera supernatant samples was put into plastic immunoplate wells and incubated at 4°C overnight. The wells were rinsed 3 times with a washing buffer (0.05% Tween 20/citrate-containing phosphate-buffered saline) and 100 μl of HRP-conjugated anti-mouse IgG antibody was added and incubated at room temperature for 1 h. The wells were rinsed 3 times with a washing buffer, and 100 μl of hydrogen peroxide/citrate containing phosphate-buffered 1% 3,3′,5,5′-tetramethylbenzidine was added. After 15 min 1 M phosphate was added to the wells to stop the reaction. The absorbance at 450 nm of the reaction mixture was measured with a microplate reader (PerkinElmer, Wellesley, Mass., USA) and a standard curve was used to determine the amount of 8-OHdG present in the test samples. The standard curve was generated by plotting absorbance versus log (concentration of standards), then the absorbance values obtained for the test samples were used to determine the concentrations [34].

Detection of HEL

The HEL levels were assessed in triplicate by HEL ELISA Kit-700 using an anti-HEL monoclonal antibody (Institute for the Control of Aging, Shizuoka, Japan). The competitive indirect ELISA was conducted as established previously with some modifications [31]. Briefly, 50 μl of the saliva samples was titrated into each well of a 96-well microtiter plate and then 50 μl of the anti-HEL monoclonal antibody solution/well was added and kept overnight at 4°C. The wells were rinsed 3 times with a washing buffer (0.05% Tween 20/citrate-containing phosphate-buffered saline) and HPR-conjugated anti-mouse IgG antibody was added and incubated at room temperature for 1 h. The wells were rinsed 3 times with a washing buffer, and hydrogen peroxide/citrate containing phosphate-buffered 1% 3,3′,5,5′-tetramethylbenzidine was added. After 15 min, the color development was stopped by the addition of 1 M phosphate into the wells. The optical density of each well was determined by a microplate reader (PerkinElmer) at 450 nm.

Detection of Lactate Dehydrogenase

Lactate dehydrogenase (LDH) concentrations in the saliva were measured in triplicate using an LDH Cytotoxicity Detection Kit (Takara Bio, Shiga, Japan). Briefly, centrifuged saliva samples were placed in a 96-well microtiter plate with diapholate/NAD^+ and 11.25 ml of iodotetrazolium chloride/Na-lactate added to each well. After 30 min, 1 N hydrochloric acid was added to the wells to stop the reaction. The absorbance of the samples was measured at 490 and 630 nm according to the filters available using an ELISA reader (PerkinElmer). The LDH concentration in the saliva was normalized to that of the control group.

Detection of Mitochondrial Glutamic-Oxaloacetic Transaminase

Activity of mitochondrial glutamic-oxaloacetic transaminase (m-GOT) was determined with a commercially available kit (Sysmex, Hyogo, Japan). β-NADH/oxaloacetate mixture (250 μl) was incubated with the samples (20 μl) for 10 min at 37°C, then the reaction was started by adding 100 μl α-ketoglutarate/L-aspartate mixture and incubated for 3 min at 37°C. The absorbance of the samples was measured at 340 nm (Hitachi 7170 Automatic Analyser, Tokyo, Japan).

Determination of Apolipoprotein B

The levels of apolipoprotein B were determined by turbidimetric immunoassay methods. The microtiter plate containing 100 mM 2-amino-2-hydroxymethyl-1,3-propanediol buffer (300 μl) was placed in a spectrophotometer and incubated for 5 min at 37°C. Anti-human apolipoprotein B polyclonal antibody was added and incubated for 5 min at 37°C. Absorbance was estimated in 2-point endpoint, at 340 and 694 nm.

Lip Biopsy Samples

The 8 patients diagnosed with SS underwent labial minor salivary gland biopsies after having given their consent. Sections from the labial minor salivary gland biopsies were stained with hematoxylin and eosin (HE) using the standard method. Three trained pathologists evaluated the focal lymphocytic infiltration in the minor salivary glands by the HE-stained section according to Greenspan's criteria [35]: grade 0: absent; grade 1: slight infiltrate; grade 2: moderate infiltrate or less than one focus per 4 mm^2; grade 3: one focus per 4 mm^2, and grade 4: more than one focus per 4 mm^2. Grades 3 and 4 were considered to be positive according to the SS criteria [36].

Statistical Analysis

Data were presented as mean ± SD and range. Comparisons between the groups were statistically analyzed by one-way analysis of variance (ANOVA) followed by Scheffé's test. Correlations between variables were assessed with Pearson's correlation coefficient. Statistical analysis of the data was carried out by using the Statview software program for the Macintosh computer. $p < 0.05$ was taken as being statistically significant.

Ethics

Informed consent was obtained from all the patients, and the Ethical Committee of the Tsurumi University approved this study.

Results

To examine whether the 8-OHdG and HEL levels in the saliva were disease-specific, a comparative evaluation was conducted among samples taken from the different groups. The SS group, in comparison with the G1, the G2 and the control groups, showed a significant difference, thus indicating the involvement of oxidative stress in the secretory dysfunction of SS (table 2). On the other hand, there was no correlation between the G1, the G2 and the control groups. Both the SS and the G1 groups are associated with reductions in salivary secretion of similar severity, but there was a significant difference in the 8-OHdG ($p < 0.0001$) (fig. 1) and the HEL ($p < 0.01$) levels (fig. 2) between these two groups. Thus it was suspected that there may be a mechanism that causes salivary gland dysfunction that is independent of oxidative stress. There are various causes of dry mouth such as side effects from medications with anticholinergic activity, diabetes mel-

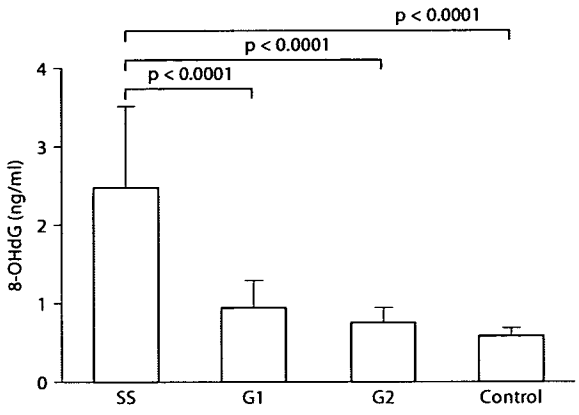

Fig. 1. 8-OHdG levels of saliva of all the groups. Values are expressed as mean ± SD. One-way ANOVA revealed a significant difference between G1, G2 and control vs. SS. $p < 0.0001$; Scheffé's test was conducted. There was no significant difference between G1, G2 and control groups. G1 vs. G2, $p = 0.9114$; G1 vs. control, $p = 0.5467$; G2 vs. control, $p = 0.8997$.

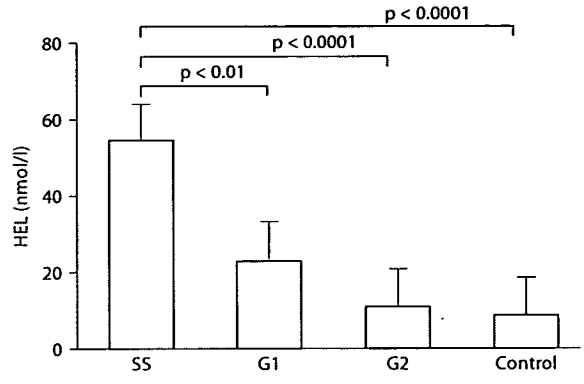

Fig. 2. HEL levels of saliva of all the groups. Values are expressed as mean ± SD. These results significantly corresponded with the increase in the 8-OHdG level in saliva. One-way ANOVA revealed a significant difference between G1 vs. SS, $p < 0.01$, and G2 and control vs. SS, $p < 0.0001$; Scheffé's test was conducted. There was no significant difference between G1, G2 and control groups. G1 vs. G2, $p = 0.4617$; G1 vs. control, $p = 0.3091$; G2 vs. control, $p = 0.9917$.

Table 2. Differences between 8-OHdG, HEL, LDH, m-GOT, and apolipoprotein B (apoB) levels (mean ± SD) in the SS group vs. G1, G2 and control groups

	SS	G1	G2	Control
Salivary 8-OHdG, ng/ml	2.5 ± 1.0	0.9 ± 0.3	0.7 ± 0.2	0.6 ± 0.1
Serum 8-OHdG, ng/ml	0.3 ± 0.1	0.2 ± 0.1	ND	0.2 ± 0.1
HEL, nmol/l	53.9 ± 25.4	22.8 ± 10.3	10.7 ± 2.3	8.4 ± 1.9
LDH, relative units	0.8 ± 0.2	0.4 ± 0.3	0.2 ± 0.1	0.1 ± 0.1
m-GOT, IU/l	79.0 ± 44.9	20.9 ± 25.8	10.9 ± 12.1	5.1 ± 1.2
apoB, mg/dl	<5	<5	<5	<5

The relative units of LDH in the saliva were normalized to that of the control group.
ND = Not determined.

litus and psychological disorders and these were possible causative factors for the salivary gland dysfunction in the G1 group.

To validate the results of the salivary analysis given above, the 8-OHdG serum level was measured in individual patients. Compared with those taken from the control group, the serum samples from the SS group exhibited a trend similar to that of the saliva samples ($p = 0.3444$) (fig. 3). This result was interpreted to support the reliability of 8-OHdG detection in the saliva of SS patients. On the other hand, it was considered possible that the 8-OHdG contained in the saliva samples might be derived from the blood circulation. However, the concentration of apolipoprotein B, a marker for serum origin, was found to be below the detectable level in the same saliva samples (table 2). Furthermore, the 8-OHdG levels in the saliva were 10-fold higher than that in the sera, thus proving that the salivary 8-OHdG was of salivary gland origin. It was assumed that the 8-OHdG in the sera detected in the SS patients was a reflection of glandular tissue damage or damage to other organs due to the response to autoimmunity.

The results described above suggested that the glandular tissue damage was caused by oxidative stress. To sub-

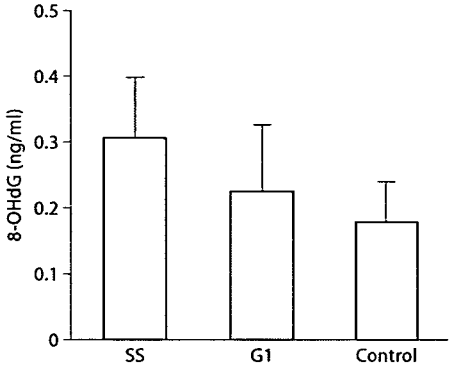

Fig. 3. 8-OHdG levels of serum of SS, G1 and control groups. Values are expressed as mean ± SD. The serum samples of the SS group exhibited a trend similar to that of the salivary samples. There was no significant difference between the three groups, $p = 0.3444$.

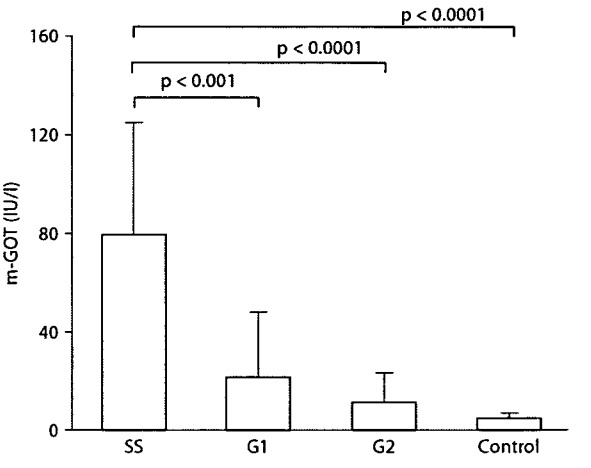

Fig. 5. m-GOT levels of saliva of all the groups. The level was significantly higher in the SS group. Values are expressed as mean ± SD. One-way ANOVA revealed significant differences between G1 vs. SS, $p < 0.001$, and G2 and control vs. SS, $p < 0.0001$; Scheffé's test was conducted. There was no significant difference between the G1, G2 and control groups. G1 vs. G2, $p = 0.8486$; G1 vs. control, $p = 0.6470$; G2 vs. control, $p = 0.9824$.

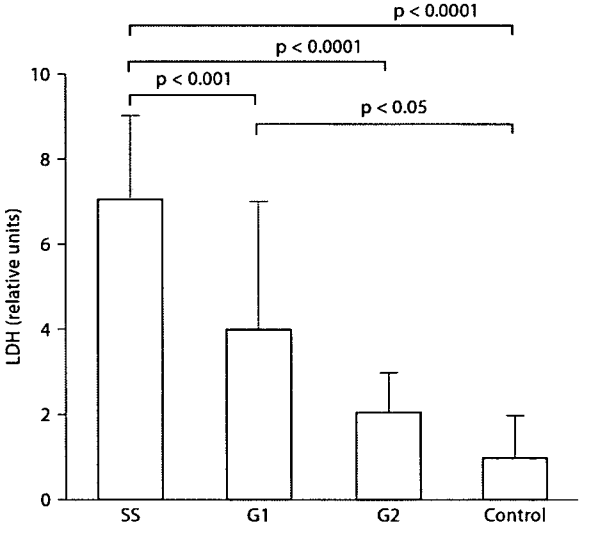

Fig. 4. LDH levels of saliva of all the groups. Values are expressed as mean ± SD. One-way ANOVA revealed significant differences between G1 vs. SS, $p < 0.001$; G2 and control vs. SS, $p < 0.0001$, and G1 vs. control, $p < 0.05$; Scheffé's test was conducted. There was no significant difference between G1, G2 and control groups. G1 vs. G2, $p = 0.4369$; G2 vs. control, $p = 0.3905$.

stantiate this further, LDH and m-GOT, which are widely employed as general markers for cell damage, were analyzed. Consequently, the LDH levels of the SS group were found to be significantly higher in comparison to those of the G1, the G2 and the control groups. There was no correlation between the G1, the G2 and the control groups (fig. 4; table 2). The m-GOT levels of the SS group were also significantly higher than those of the other groups, generally duplicating the pattern seen in the 8-OHdG levels, but there was no correlation between the G1, the G2 and the control groups (fig. 5; table 2). In all the groups, the LDH and m-GOT levels significantly correlated with the 8-OHdG and HEL levels (fig. 6). Furthermore, the 8-OHdG and HEL levels were also correlated ($r = 0.8971$, $p < 0.0001$) (fig. 7).

Next, the correlation between the extent of tissue damage expressed by the salivary markers and the results of the histopathological evaluation of SS was examined. There was no marked correlation between the histological grade and the levels for 8-OHdG ($p = 0.8231$) and HEL ($p = 0.5485$; data not shown). We speculate that this may be explained through the fact that oxidative stress is a causative agent for not only destruction, but also cellular dysfunction by oxidative degeneration of lipid membranes and membrane proteins [37].